2002

Nonlinear device characterization using harmonic load pull measurement

Atiwat Aimdilokwong
Iowa State University

INFORMATION TO USERS

This manuscript has been reproduced from the microfilm master. UMI films the text directly from the original or copy submitted. Thus, some thesis and dissertation copies are in typewriter face, while others may be from any type of computer printer.

The quality of this reproduction is dependent upon the quality of the copy submitted. Broken or indistinct print, colored or poor quality illustrations and photographs, print bleedthrough, substandard margins, and improper alignment can adversely affect reproduction.

In the unlikely event that the author did not send UMI a complete manuscript and there are missing pages, these will be noted. Also, if unauthorized copyright material had to be removed, a note will indicate the deletion.

Oversize materials (e.g., maps, drawings, charts) are reproduced by sectioning the original, beginning at the upper left-hand corner and continuing from left to right in equal sections with small overlaps.

Photographs included in the original manuscript have been reproduced xerographically in this copy. Higher quality 6" x 9" black and white photographic prints are available for any photographs or illustrations appearing in this copy for an additional charge. Contact UMI directly to order.

ProQuest Information and Learning
300 North Zeeb Road, Ann Arbor, MI 48106-1346 USA
800-521-0600

Nonlinear device characterization using harmonic load pull measurement

by

Atiwat Aimdilokwong

A dissertation submitted to the graduate faculty

in partial fulfillment of the requirements for the degree of

DOCTOR OF PHILOSOPHY

Major: Electrical Engineering (Electromagnetics)
Program of Study Committee:
Robert J. Weber, Major Professor
David T. Stephenson
Randall L. Geiger
John R. Schroeter
Scott W. Hansen

Iowa State University

Ames, Iowa

2002

UMI Number: 3051445

UMI Microform 3051445

ProQuest Information and Learning Company
300 North Zeeb Road
P.O. Box 1346
Ann Arbor, MI 48106-1346

Graduate College
Iowa State University

This is to certify that the doctoral dissertation of

Atiwat Aimdilokwong

has met the dissertation requirements of Iowa State University

Signature was redacted for privacy.

Major Professor

Signature was redacted for privacy.

For the Major Program

DEDICATION

To my loving parents,

Prakorb and Janya Aimdilokwong

TABLE OF CONTENTS

TABLE OF FIGURES vi

TABLE OF TABLES vii

ACKNOWLEDGEMENTS viii

1. INTRODUCTION 1

1.1 Research Objective 1
1.2 Approach 2

2. HARMONIC SOURCE/LOAD PULL SYSTEM 3

3. LARGE SIGNAL CHARACTERIZATION 6

3.1 Large Signal Scattering Parameters Model 6
3.2 Equivalent Nonlinear Circuit Model 7
3.3 Direct Measurement Data Model 7
3.4 Conversion Matrix Model 7
3.4.1 Theory 9

4. MEASUREMENT THEORY 12

4.1 Large Signal Scattering Parameters Measurement 13
4.1.1 Theory 14
4.2 Multi-Harmonic Load Pull Measurement 16

5. PROCEDURE, SETUP AND RESULT 18

5.1 Setup Harmonic Source/Load Pull System to Characterize Microwave Devices 18
5.1.1 Test and Verify the Functionality of the Fixture 18
5.1.2 Characterize the Fixture 18
5.1.3 Write a Program to Deembed the Device 19
5.1.4 Test the 1st 2nd and 3rd Harmonics 19
5.2 Effect of Harmonic Load Pull on a 1W Bipolar Part 20
5.3 Effect of Half Frequency Instability on a 1W Bipolar Part 21
5.3.1 Measurement Setup 21
5.3.2 Large Signal Scattering Parameters 22
5.3.3 Half Frequency Stability 24
5.3.4 Summary 28
5.4 Effect of the Harmonic Source/Load Pull on PHEMT at 0.5 GHz 28
5.4.1 PHEMT Measurement Setup 28
5.4.2 Output Harmonic Tuning 29
5.4.3 Input Harmonic Tuning 30
5.4.4 Conclusion 32
5.5 Large Signal Scattering Parameters of The PHEMT Part at 1 GHz 32
5.5.1 PHEMT Measurement Setup 32
5.5.2 Large Signal Scattering Parameter Result 33

5.5.3 Conclusion *34*
5.6 Conversion Matrix of The PHEMT Part at 1 GHz 34
5.6.1 PHEMT Measurement Setup *34*
5.6.2 Conversion Matrix Result *34*
5.6.3 Conclusion *36*

6. APPENDIX **37**

6.1 Characteristic of 1-2-3 GHz Diplexer 37
6.2 Characteristic of 0.5-1 GHz Diplexer 40
Characteristic of the Frequency Doubler 42
6.4 Characteristic of the Fixture of the Bipolar Part 43
6.5 Characteristic of the Fixture of the PHEMT Part 45
6.6 Coupler File 46

7. BIBLIOGRAPHY **49**

TABLE OF FIGURES

FIGURE 2-1 CROSS-SECTION OF A DOUBLE-SLUG TUNER 3
FIGURE 2-2 EQUIVALENT CIRCUIT OF A DOUBLE-SLUG TUNER 4
FIGURE 2-3 SIMPLE HARMONIC LOAD PULL SETUP 5
FIGURE 4-1 SETUP FOR MEASURING LARGE SIGNAL SCATTERING PARAMETERS 14
FIGURE 4-2 SETUP FOR MEASURING CONVERSION MATRIX 17
FIGURE 5-1 BASIC SCHEMATIC OF A BIAS CONTROLLER OF THE BIPOLAR PART 18
FIGURE 5-2 BASIC SCHEMATIC OF A DIPLEXER 19
FIGURE 5-3 SECOND AND THIRD HARMONIC EFFECTS ON FUNDAMENTAL LOAD GAMMA 20
FIGURE 5-4 LOAD PULL MEASUREMENT SETUP 21
FIGURE 5-5 HALF FREQUENCY TEST SETUP 22
FIGURE 5-6 SCHEMATIC OF THE BIAS CONTROLLER FOR ADJUSTING GATE VOLAGE 29
FIGURE 5-7 OUTPUT HARMONIC TUNING SETUP 30
FIGURE 5-8 INPUT HARMONIC TUNING SETUP 31
FIGURE 5-9 SETUP FOR MEASURING LARGE SIGNAL SCATTERING PARAMETERS 33
FIGURE 6-1 CHARACTERISTIC BETWEEN INPUT PORT AND FUNDAMENTAL PORT 37
FIGURE 6-2 CHARACTERISTIC BETWEEN THE INPUT PORT AND THE SECOND HARMONIC PORT 38
FIGURE 6-3 CHARACTERISTIC BETWEEN THE INPUT PORT AND THE THIRD HARMONIC PORT 39
FIGURE 6-4 RESPONSE OF THE DIPLEXER FILTER 40
FIGURE 6-5 RESPONSE IN THE PASS BANDS FOR THE DIPLEXER 41
FIGURE 6-6 RELATIVE RESPONSES OF THE FUNDAMENTAL 42
FIGURE 6-7 CHARACTERISTIC OF THE LEFT HALF OF THE FIXTURE 43
FIGURE 6-8 CHARACTERISTIC OF THE RIGHT HALF OF THE FIXTURE 44
FIGURE 6-9 CHARACTERISTIC OF THE PHEMT FIXTURE 45

TABLE OF TABLES

TABLE 5-1 LARGE SIGNAL SCATTERING PARAMETERS OF THE BIPOLAR PART 23
TABLE 5-2 STABILITY FACTORS ON THE BIPOLAR PART 23
TABLE 5-3 SCATTERING PARAMETERS OF A BIPOLAR PART AT 500 MHZ SMALL SIGNAL 24
TABLE 5-4 STABILITY OF A BIPOLAR PART AT 500 MHZ SMALL SIGNAL 24
TABLE 5-5 SCATTERING PARAMETERS AT 0.5 GHZ WITH THE PART EXCITED SMALL SIGNAL AT 1 GHZ 25
TABLE 5-6 STABILITY AT 0.5 GHZ WITH THE PART EXCITED AT 1 GHZ SMALL SIGNAL 25
TABLE 5-7 SCATTERING PARAMETERS AT 0.5 GHZ WITH THE PART EXCITED LARGE SIGNAL AT 1 GHZ 26
TABLE 5-8 STABILITY AT 0.5 GHZ WITH THE PART EXCITED LARGE SIGNAL AT 1 GHZ 26
TABLE 5-9 SCATTERING PARAMETERS AT 0.5 GHZ WITH THE PART OVER DRIVEN AT 1 GHZ 27
TABLE 5-10 STABILITY AT 0.5 GHZ WITH THE PART OVER DRIVEN AT 1 GHZ 27
TABLE 5-11 EFFECT OF OUTPUT TUNING ON POWER OUTPUT 30
TABLE 5-12 EFFECT OF INPUT TUNING ON POWER OUTPUT 31
TABLE 5-13 SMALL SIGNAL AND LARGE SIGNAL SCATTERING PARAMETERS OF TWO PHEMTS 34
TABLE 6-1 COUPLER FILE (PART 1) 46
TABLE 6-2 COUPLER FILE (PART 2) 47
TABLE 6-3 COUPLER FILE (PART 3) 48

ACKNOWLEDGEMENTS

I would like to thank my major professor, Dr. Robert J. Weber, for providing me guidance and encouragement throughout the time that I have been at Iowa State University. I also thank him for providing financial support through research assistantships and teaching assistantships. Time domain waveform measurements were done using a sampling oscilloscope from the Carver High Speed Communications Laboratory. The laboratory was set up in part by a grant from the Roy J. Carver Charitable Trust.

I also would like to thank all my friends who have given me much encouragement. They are in various places: in the same laboratory, in Florida, at Campus Baptist Church. I am grateful for everyone in my family who has given me help and support in every way.

1. INTRODUCTION

There has been a large amount of work and effort going on in the area of high and medium power MMICs (Monolithic Microwave Integrated Circuits) recently. Today nonlinear microwave active devices such as power amplifiers can still benefit from better performance (such as power output and efficiency) by having suitable terminations at various harmonic frequencies. On the other hand, sub-harmonic terminations can affect the stability of the device. The main reason lies in the nonlinear behavior of the device that causes the device to generate various harmonic frequencies apart from the fundamental frequency.

Harmonic Balance (HB), [Nakhla, 1976][Rizzoli, 1988][Gilmore 1991] has been a widely used and by far the most popular method to solve for a steady state solution of a nonlinear microwave circuit. It is done by splitting the nonlinear circuit into two parts: a linear part consisting of all the linear circuit elements and a nonlinear part consisting of all the nonlinear circuit elements. Voltages and currents at a number of ports at the interface between the linear part and nonlinear part are then computed and matched together using Kirschoff's voltage and current law. The result is a solution for the voltages and currents and their harmonics at all the ports. In order to use the harmonic balance method, we need some characterization or model of both the linear part and the nonlinear part. We already have a very good characterization in form of governing equations for the linear part (such as transmission lines, linear resisters, capacitors and inductors). That is not true for the nonlinear active device operating at a large signal level. We still lack a good and sound characterization method for the nonlinear device. This is what we are set to do in this paper. We use a large signal harmonic source/load pull system to present a variety of input and output terminations to the nonlinear device and while doing that we make measurements of some parameters (such as current, voltage or power variables) of the nonlinear device. We make use of the measured data to come up with a large signal characterization of the nonlinear device that gives the relationship between signals at various frequencies (harmonics) in addition to the frequency of interest.

1.1 Research Objective

This research objective is to investigate and characterize the nonlinear behavior of microwave devices by using harmonic source/load pull system measurements. From a measurement, the large signal conversion matrix or other equivalent method, which tells the relationship of parameters (such as S, Z or Y) of the device, between the fundamental frequency and the harmonic frequencies, will be realized.

1.2 Approach

In order to characterize the nonlinear microwave devices, one needs to be able to measure both magnitude and phase of the harmonic signals being generated. There are many ways of obtaining the information (e.g. magnitude and phase) of the harmonic signals of interest. If we can get both the magnitude and phase of the signals at the fundamental frequency and the harmonic frequencies, then the conversion matrix describing the nonlinear device characteristic can be obtained.

The network analyzer is useful for measurement of the scattering parameters of a linear small signal microwave circuit. In order to characterize a nonlinear device, the network analyzer has to be able to measure both the signal at the fundamental frequency and the signals at the harmonic frequencies. The network analyzer HP8753C that we have has the harmonic add-on option but it does not work as we first thought. The network analyzer in the harmonic mode does not measure the phase relationships between the fundamental and the harmonic frequencies. Instead the measurement is done within the same harmonic frequency only so we could not get the phase reference between the signal at the fundamental frequency and the signals at the harmonic frequencies. In addition to that it measures the harmonic signal with respect to the residue harmonic signal inside the network analyzer itself not the harmonic signals that we want at the device ports.

Since we cannot get a correct magnitude and phase measurement between the fundamental frequency and the harmonic frequencies from the network analyzer, other alternatives are considered in this research. This is discussed in detail in "Measurement System" chapter.

After obtaining the correct magnitude and phase information at the fundamental frequency and the harmonic frequencies, the conversion matrix can be obtained. From the conversion matrix, one should be able to predict how the input and output harmonic terminations are going to affect the performance of the nonlinear device. In summary, the nonlinear characterization of the bipolar transistor or the PHEMT (Psuedo-morphic High Electron Mobility Transistor) using the conversion matrix will be performed.

2. HARMONIC SOURCE/LOAD PULL SYSTEM

Source/Load pull measurement [Takayama, 1976] is a very popular method for characterizing the large signal characteristic of nonlinear two-port devices such as microwave transistors. The measurement is accomplished by placing tunable terminations on the input and output of the device. Usually the device is biased at some operating point and data are gathered at various input and output terminations. The advantage of source/load pull measurement is that it is usually a very reliable and repeatable measurement. There are two types of source/load pull measurement. One is passive source/load pull and the other is active source/load pull. The passive source/load pull, [Sechi, 1983] can be done using impedance-transforming tuners to present suitable impedances to the two-port device. The most common type is the double-slug tuner. The tuner, shown in Figure 2-1, operates by having a 50Ω transmission line surrounded by a series of two slugs with a fixed distance between them. The two slugs are designed to induced a mismatch in the transmission line. The vertical position of each slug can be adjusted individually. The horizontal position between the slugs is constant. The slugs move together along the transmission line (we call this the carriage position). The two slugs are different in their sizes. One slug will be bigger than the other. This will help the tuner to be able to adjust its input impedance over a wider frequency range. The two-slug tuner can be modeled as cascaded transmission lines of different characteristic impedances and time delays as shown in Figure 2-2.

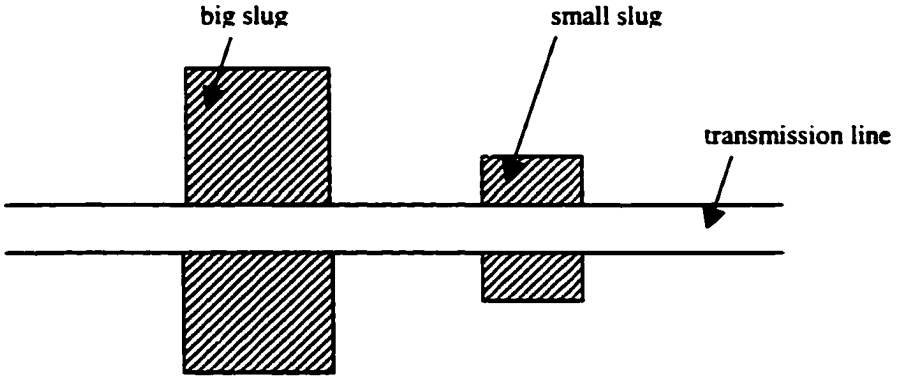

Figure 2-1 Cross-section of a double-slug tuner

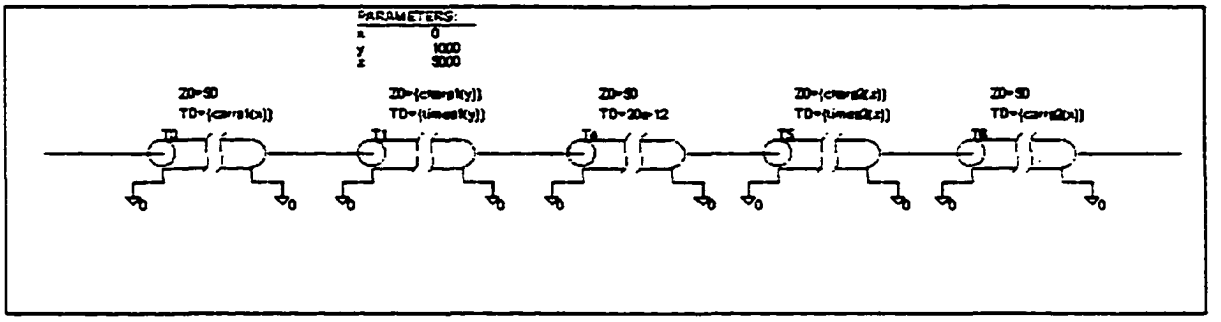

Figure 2-2 Equivalent circuit of a double-slug tuner

The active source/load pull measurement [Takayama, 1976] differs from the passive source/load pull measurement in that it uses a waveform shaping mechanism that injects signals directly to the device, presenting an impedance to the two-port device and hence the name active source/load pull. It has some advantages over the passive source/load pull because it can present a more accurate and wider range of impedance to the two-port device because it does not have the transmission line losses of the tuner. It is also considered faster because it does not have to physically move the slugs as in the case of the passive source/load pull.

The system that we use is the passive type. We use passive tuners to present different impedances to the nonlinear device. However we have one tuner for each frequency on the input and output port of the device and this is called the harmonic source/load pull [Heymann, 2000][Cai, 1998]. In order to make each frequency distinct to the tuners, we use a frequency multiplexer. Usually this is called a diplexer for a two-frequency case. A simple setup for doing a harmonic load pull measurement is shown in Figure 2-3.

Conventional harmonic source/load pull measurement is done by measuring the power output at the fundamental frequency and the harmonic frequencies as the terminations are varied by means of tuners. Usually the power output at the fundamental frequency is of interest. Usually before we can make harmonic source/load pull measurements, the following steps need to be performed and tested.

- Build and test the fixture. This includes the bias control circuit.
- Characterize the fixture and verify its functionality.
- De-embed the device to get the parameters at the device plane instead of at the end of the fixture using data from the device characterization.

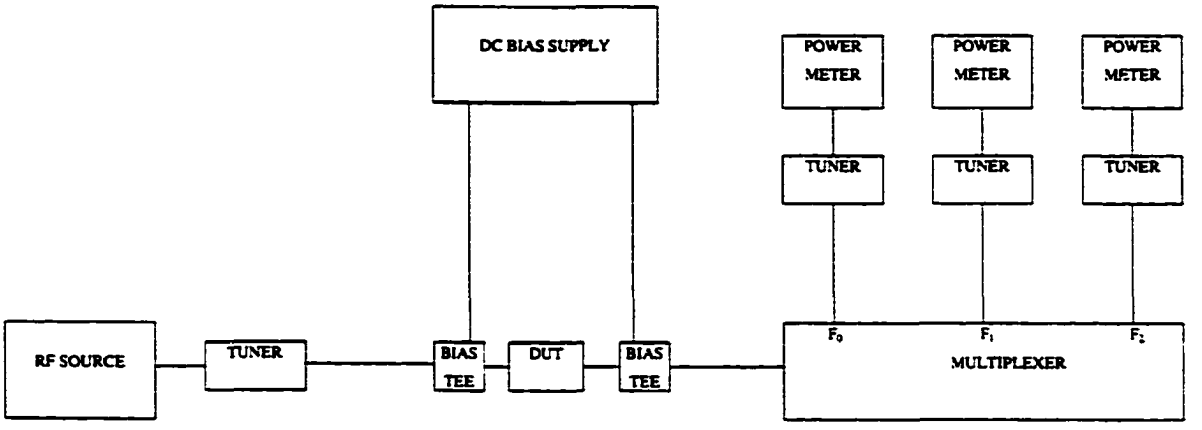

Figure 2-3 Simple harmonic load pull setup

3. LARGE SIGNAL CHARACTERIZATION

In the past, there has been a variety of large signal characterizations of the nonlinear two-port device. Many attempts have been made to characterize the device by resorting to the large signal scattering parameter measurement [Mazumder, 1978]. Large signal - small signal conversion matrices [Maas, 1988] and Volterra Series [Maas, 1988][Chua, 1972][Hu, 1989] are also used to characterize the nonlinear behavior of the device. A lot of effort was also made to build an equivalent large signal nonlinear circuit model [Teeter, 1993][Ebers, 1954][Chang, 1986][Curtice, 1985][Materka, 1985] of the device. In our attempt, we characterize the large signal nonlinear behavior of the device by a large signal conversion matrix that is computed from direct measurement data. This can be compared to a widely used technique in microwave engineering, which uses a measured set of small signal scattering parameters of the device as a way to characterize it without having to build an equivalent circuit model.

3.1 Large Signal Scattering Parameters Model

The idea of large signal scattering parameter measurement is same as that of the well established small signal scattering parameter measurement, that is measuring the ratio of power variables at the ports of the device on a swept frequency basis. The small signal scattering parameters can be of good use in the linear operating region of the device but when the input power goes up, eventually the active device will go into nonlinear region. When this happens, the active device will be nonlinear and the scattering parameter measurement will be dependent on the power level. In order to get a complete set of large signal scattering parameters, the measurement needs to be done on both swept frequency basis and swept power basis. There is an inherent problem with the large signal scattering parameters, that is the large signal scattering parameters are usually only good for terminations that are used during measurement. This problem comes from the dependence of large signal scattering parameters on the power level because when we change the load termination, this affects the power level. This has to do with the relationship between output power and the position of the load termination on the load line of the nonlinear device. Also at a large signal drive, the device will create harmonic frequencies so we are required to think of the large signal scattering parameters in terms of a matrix of scattering parameters relating power variables at various harmonic frequencies. In the following section, this leads to the idea of using a large signal conversion matrix to characterize the nonlinear device.

3.2 Equivalent Nonlinear Circuit Model

The nonlinear circuit model has been a popular technique to characterize the nonlinear microwave device in the past. A fair amount of knowledge of how the nonlinear device operates is needed. There are some nonlinear circuit models available for some transistors already such as the Gummel Poon Model [Teeter, 1993], Modified Ebers Moll Model [Cai, 1998], Curtice and Ettenger model [Curtice, 1985], and Modified Materka Model [Materka, 1985]. Somehow, an identification procedure is needed to extract all the values in the model from the measurement. After all the values in the model are known, then the model has to be tested to see if it agrees with the large signal and small signal performance of the device. Nonlinear Models are sometimes useful to gain insight into the physical behavior of the device. Unfortunately, nonlinear models are not always accurate over a wide range of large signal level.

3.3 Direct Measurement Data Model

There are various kinds of models obtained directly from measurement data. Some have been implemented in the microwave simulation program ADS v1.50 [ADS, v1.50]. For example, the data models can be from the load pull measurement data or the amplifier's fundamental and second harmonic signals vs. input power. This method is similar to a database approach since the simulation will perform a table lookup from the data files and find the device characteristic at that operation point.

3.4 Conversion Matrix Model

This method is very similar to small signal linear scattering parameters except that instead of getting just scattering parameters, we get matrices instead. Each element in the matrix relates to the interaction between harmonics of the device. The device is usually pumped with a large signal at a frequency. The pump signal is large enough to drive the device into nonlinear regions of operation and thus create harmonics. Then the characterization of the device is evaluated at some frequency by injecting a small signal at that frequency. This gives the small signal conversion matrix when the device is pumped with a large signal at another frequency. The conversion matrix is useful to characterize devices such as mixers and parametric amplifiers, which operate with large signal – small signal at the same time.

To apply this method to an active nonlinear device such as power amplifiers, we need to develop a large signal conversion matrix. We need the large signal conversion matrix because the nonlinear device such as power amplifiers usually operate at only one frequency and that signal is large enough to create harmonic

frequencies but there are often no mixings between this large signal and some small signals as in the case of mixers.

From the relationship of the linear two-port scattering parameters [Kurokawa, 1965], we have the following

$$\begin{bmatrix} b_1 \\ b_2 \end{bmatrix} = \begin{bmatrix} s_{11} & s_{12} \\ s_{21} & s_{22} \end{bmatrix} \cdot \begin{bmatrix} a_1 \\ a_2 \end{bmatrix} \tag{3-1}$$

For the nonlinear device, the scattering parameters are nonlinear and can be expressed as a Fourier series with terms according to the harmonics. The power waves "a" and "b" now have components at harmonic frequencies.

$$\begin{bmatrix} B_1 \\ B_2 \end{bmatrix} = \begin{bmatrix} S_{11} & S_{12} \\ S_{21} & S_{22} \end{bmatrix} \cdot \begin{bmatrix} A_1 \\ A_2 \end{bmatrix} \tag{3-2}$$

The "A" and "B" represent vectors of the power waves "a" and "b" at fundamental and various harmonic frequencies. The "S" represents the matrix that relates the power wave vectors "A" and "B" together. We call this individual "S" matrix a "Conversion Matrix" because it relates to the conversion of various frequencies in the power wave vectors "A" and "B" together.

In order to find this conversion matrix, we have to limit the harmonic frequencies that we are interested in. Assume that the device is nonlinear up to the second harmonic (meaning that it generates an insignificant amount of higher order harmonic frequencies), each power wave vector "A" and "B" will be a vector of length 4 if we include the negative frequencies as well. Then each "S" matrix will be of size 4x4. Now we can write this

$$\begin{bmatrix} B_1 \\ B_2 \end{bmatrix}_{8x1} = \begin{bmatrix} S_{11} & S_{12} \\ S_{21} & S_{22} \end{bmatrix}_{8x8} \cdot \begin{bmatrix} A_1 \\ A_2 \end{bmatrix}_{8x1} \tag{3-3}$$

From this conversion matrix, we should be able to predict how the input and output harmonic terminations are going to affect the performance of the nonlinear device.

3.4.1 Theory

In order to investigate the relationship between the harmonic signals generated in a nonlinear device operating under large signal condition, a conversion matrix is formulated. The conversion matrix is developed from the perturbation of the large signal that the device is operating at. When the device operates under the large signal condition, a number of frequencies (harmonics) are generated. The conversion matrix is actually the slope (or the Jacobian matrix for multi-dimensional case) of the actual nonlinear relationship governing the device. The conversion matrix thus will not work over a large range of signal level but it is useful for predicting the effect of harmonic terminations on efficiency, stability and intermodulation distortion at that particular large signal level. The usefulness of the conversion matrix for intermodulation phenomena, especially the requirement for input and output load terminations in a PHEMT device can be further investigated if time permits.

Currently conversion matrix theory is not generally applied to large signal circuits. This can be investigated whether the measured conversion matrix allows its application to large signal circuits by making the measurements in regions where there is not a lot of variation of the large signals. This should be similar to the small signal case where the variation is from a zero signal case except we would be varying by a small signal from a large signal case.

Consider a case of the perturbation of the large signal nonlinear relationship of a simple nonlinear conductance I = G(V). This can be written as

$$i(t) = g(t).v(t) \tag{3-4}$$

Then g(t) can be expressed in terms of Fourier series with terms according to the harmonics

$$g(t) = \sum_{n=-\infty}^{\infty} g_n e^{jn\omega_0 t} \tag{3-5}$$

The voltage and current waveform can also be expressed as functions of harmonic frequencies

$$v(t) = \sum_{n=-\infty}^{1} v_n e^{jn\omega_0 t} + \sum_{n=1}^{\infty} v_n e^{jn\omega_0 t}$$
$$i(t) = \sum_{n=-\infty}^{1} i_n e^{jn\omega_0 t} + \sum_{n=1}^{\infty} i_n e^{jn\omega_0 t}$$

(3-6)

where $v_{-n} = v_n^*$
$i_{-n} = i_n^*$

because v(t) and i(t) are real functions. Putting equations (3-5) and (3-6) in (3-4) and matching the terms according to the harmonic frequencies, the relationship can be written in a matrix form. For example, consider the harmonic frequencies up to the third order

$$\begin{bmatrix} i_{-3} \\ i_{-2} \\ i_{-1} \\ i_1 \\ i_2 \\ i_3 \end{bmatrix} = \begin{bmatrix} g_0 & g_{-1} & g_{-2} & g_{-4} & g_{-5} & g_{-6} \\ g_1 & g_0 & g_{-1} & g_{-3} & g_{-4} & g_{-5} \\ g_2 & g_1 & g_0 & g_{-2} & g_{-3} & g_{-4} \\ g_4 & g_3 & g_2 & g_0 & g_{-1} & g_{-2} \\ g_5 & g_4 & g_3 & g_1 & g_0 & g_{-1} \\ g_6 & g_5 & g_4 & g_2 & g_1 & g_0 \end{bmatrix} \begin{bmatrix} v_{-3} \\ v_{-2} \\ v_{-1} \\ v_1 \\ v_2 \\ v_3 \end{bmatrix}$$

(3-7)

Assuming the device is non-linear up to the second order then we can rewrite the matrices as

$$\begin{bmatrix} i_{-3} \\ i_{-2} \\ i_{-1} \\ i_1 \\ i_2 \\ i_3 \end{bmatrix} = \begin{bmatrix} g_0 & g_{-1} & g_{-2} & 0 & 0 & 0 \\ g_1 & g_0 & g_{-1} & 0 & 0 & 0 \\ g_2 & g_1 & g_0 & g_{-2} & 0 & 0 \\ 0 & 0 & g_2 & g_0 & g_{-1} & g_{-2} \\ 0 & 0 & 0 & g_1 & g_0 & g_{-1} \\ 0 & 0 & 0 & g_2 & g_1 & g_0 \end{bmatrix} \begin{bmatrix} v_{-3} \\ v_{-2} \\ v_{-1} \\ v_1 \\ v_2 \\ v_3 \end{bmatrix}$$

(3-8)

This is redundant because the negative and positive frequency components are complex conjugate of another. Without loss of generality, the relationship can be further simplified.

$$\begin{bmatrix} i_1 \\ i_2 \\ i_3 \end{bmatrix} = \begin{bmatrix} g_0 & g_{-1} & g_{-2} \\ g_1 & g_0 & g_{-1} \\ g_2 & g_1 & g_0 \end{bmatrix} \cdot \begin{bmatrix} v_1 \\ v_2 \\ v_3 \end{bmatrix}$$

(3-9)

As the circuit gets more complicated, the conversion matrix in equation (3-8) will change form. The components inside the conversion matrix will all have different values (e.g. not having the same value along the diagonal axis anymore) since the components are frequency dependent also unlike a simple conductance. For microwave device, the scattering parameters are preferred over voltage and current. From the definition of the scattering parameters in equation (3-10), one can rewrite it in terms of the conversion matrix in equation (3-11). The second subscript ij (after a comma) in the conversion matrix refers to the causal relationship of the j^{th} harmonic to the i^{th} harmonic.

$$\begin{bmatrix} b_1 \\ b_2 \end{bmatrix} = \begin{bmatrix} s_{11} & s_{12} \\ s_{21} & s_{22} \end{bmatrix} \cdot \begin{bmatrix} a_1 \\ a_2 \end{bmatrix}$$

(3-10)

$$\begin{bmatrix} b_{1,1} \\ b_{1,2} \\ b_{2,1} \\ b_{2,2} \end{bmatrix} = \begin{bmatrix} s_{11,11} & s_{11,12} & s_{12,11} & s_{12,12} \\ s_{11,21} & s_{11,22} & s_{12,21} & s_{12,22} \\ s_{21,11} & s_{21,12} & s_{22,11} & s_{22,12} \\ s_{21,21} & s_{21,22} & s_{22,21} & s_{22,22} \end{bmatrix} \cdot \begin{bmatrix} a_{1,1} \\ a_{1,2} \\ a_{2,1} \\ a_{2,2} \end{bmatrix}$$

(3-11)

4. MEASUREMENT THEORY

Vectorial network analyzers are very common today and can help us characterize accurately the linear microwave networks/devices in terms of scattering parameters. This is done individually at each frequency of interest and scattering parameters are phasor terms in the frequency domain. For nonlinear devices such as microwave power amplifiers, the characterization done at each frequency separately is not suited and does not give an accurate characteristic of that device, because vectorial network analyzer use only sine waves at a frequency of interest and nonlinear devices exhibit a lot of harmonic signals.

The network analyzer HP8753C has harmonic capability. This means that it should be able to measure the transfer characteristics between harmonic and fundamental frequencies. Unfortunately after a detailed investigation, it turns out that the network analyzer does not measure the correct relationships between the fundamental frequency and the harmonic frequencies. It turns out that the measurement is done within the same harmonic frequency only. That means we could not get the correct phase reference between the signal at the fundamental frequency and the signals at the harmonic frequencies. In addition to that it measures the harmonic signal with respect to an internal harmonic signal inside the network analyzer itself instead of the incident harmonic signal on the device. The measurement can provide meaningful result if the circuitry inside the HP8753C is known. A good calibration is also needed. However, we could not get help from Agilent regarding the harmonic mode operation inside the HP8753C.

In order to extend the capabilities of the network analyzer, many ideas are proposed to help measure both magnitude and phase of the harmonic signals generated in nonlinear microwave devices. Lott [Lott, 1989] used a reference diode in place of the device to calibrate phase of the harmonic signals. Measurement was accomplished by a network analyzer being phased locked to a signal generator with an internal multiplier. Verspecht [Verspecht, 1995] and Barataud [Barataud, 1999] measured the harmonic signals both at the input and output port of the microwave device. A broadband downconverter and an intermediate frequency (IF) digitizer are used to measure the harmonic signals. The calibration was also accomplished by using a reference diode (SRD). The equipment called "Microwave Transition Analyzer" [Browne, 1991] is built based on this broadband downconverter concept. The Microwave Transition Analyzer is a sampler-based instrument. It can perform vector measurement (magnitude and phase) at the frequency of interest. This is done by the harmonic repetitive sampling technique. It samples the time waveform of the signal and performs the Fourier transform on the signal. Kompa [Kompa, 1990] and Sipila [Sipila, 1988] both utilized sampling oscilloscopes for waveform measurement and error correction in their measurement. The high speed sampling oscilloscope offers a practical solution for waveform measurement and thus characterization of nonlinear devices. It samples collectively various parts of the voltage waveform from many cycles and combines them together to get one complete cycle

of the waveform. The main difference between a microwave transition analyzer and a sampling oscilloscope is that a microwave transition analyzer triggers on the signal after it has been sampled and filtered whereas a sampling oscilloscope triggers directly on the high-speed signal itself. In addition, the sample rate (20 Msample/s) of a microwave transition analyzer is faster than that of a sampling oscilloscope (2 KSample/s). At the time of this research, however, we cannot get access to this microwave transition analyzer so the sampling oscilloscope, Agilent 86100A, will be used in this research.

4.1 Large Signal Scattering Parameters Measurement

A setup using large signal load pull is used here in Figure 4-1 instead of the conventional 50Ω terminations as used in small signal scattering parameter measurement. Two dual directional couplers are used in the setup. The network analyzer (also used as an RF source) is set to measure S21, the forward transfer characteristic between port "0" and ports "3", "4", "7" and "8". These are the reflected power waves b3, b4, b7 and b8 respectively since the ports "3", "4", "7" and "8" are matched to a 50Ω termination. Another alternative is to use sampling oscilloscope to measure the voltage waveform at ports "3", "4", "7" and "8". These voltage waveforms can be Fourier transformed to extract the fundamental components of the reflected power waves b3, b4, b7 and b8 respectively. First the source and load tuners are tuned to find the optimum source and load impedance. At the optimum source and load terminations, we perturbed the load impedance by a tuning the load tuner by a small amount in the direction radially and tangentially in the load gamma plane. We choose nine points to determine the scattering parameters of the device at maximum power. Three points were at the maximum magnitude of gamma, three points at a slightly smaller magnitude of gamma and three more points at again a smaller magnitude of gamma. The scattering parameters that result from these movements were very similar to each other but there are some differences. These differences can show instabilities as the loads are tuned either in the tangential or radial direction. These nine points are numbered

1 2 3
4 5 6
7 8 9

Point 5 is the load termination that gives maximum power. The points in the same row are at the same magnitude of gamma but their angles are displaced by a few degrees. The points in the same column are at the same angle but the magnitudes of gamma are different.

At each point of the nine load gamma positions, S21 is measured between ports "0"-"3", "0"-"4", "0"-"7" and "0"-"8" but any two points could be used to generate a large signal scattering parameter matrix.

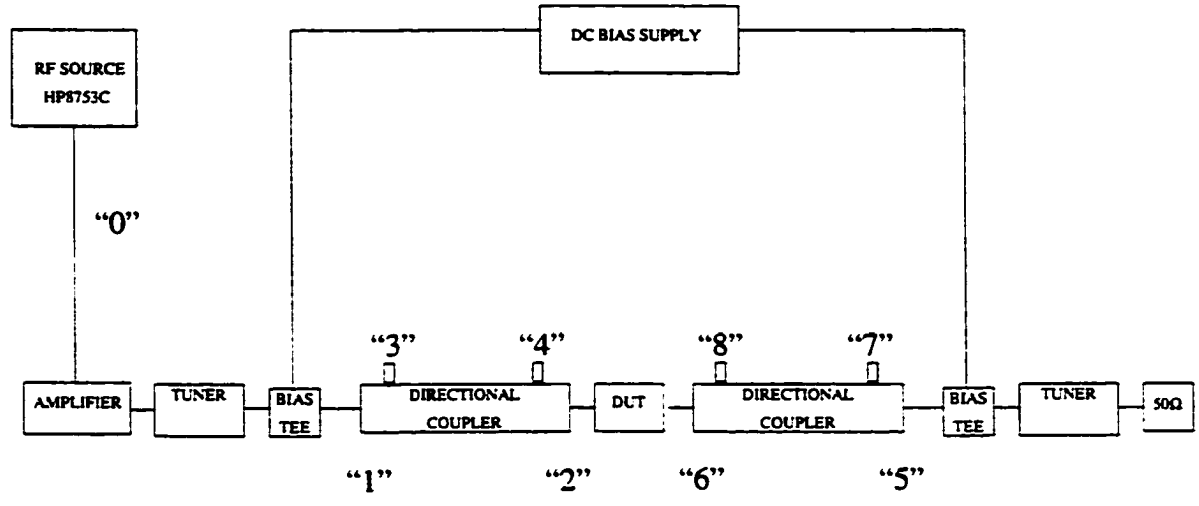

Figure 4-1 Setup for measuring large signal scattering parameters

4.1.1 Theory

Consider the input dual directional coupler. The four port scattering parameters can be measured easily using the network analyzer as shown in equation (4-1). Ports "3" and "4" are always matched at 50Ω as they are connected to the network analyzer during the S21 measurement. Then a3 and a4 are always zero as shown in equations (4-2) and (4-3). From equation (4-3), we use the matrix inverse to find a1 and a2 as in equation (4-4). Then b1 and b2 can be found in equation (4-5).

We can get a2 and b2 from the measured b3 and b4 as in equations (4-4) and (4-5) and the same can be done on the output coupler. Now we have all four power waves (a2, b2, a6, b6) at the device plane. These power waves (a2, b2, a6, b6) are now renamed (b1, a1, b2, a2) as used in equation (4-6).

$$\begin{bmatrix} b_1 \\ b_2 \\ b_3 \\ b_4 \end{bmatrix}_C = \begin{bmatrix} s_{11} & s_{12} & s_{13} & s_{14} \\ s_{21} & s_{22} & s_{23} & s_{24} \\ s_{31} & s_{32} & s_{33} & s_{34} \\ s_{41} & s_{42} & s_{43} & s_{44} \end{bmatrix}_C \cdot \begin{bmatrix} a_1 \\ a_2 \\ a_3 \\ a_4 \end{bmatrix}_C \tag{4-1}$$

$$\begin{bmatrix} b_1 \\ b_2 \end{bmatrix}_C = \begin{bmatrix} s_{11} & s_{12} \\ s_{21} & s_{22} \end{bmatrix}_C \cdot \begin{bmatrix} a_1 \\ a_2 \end{bmatrix}_C \tag{4-2}$$

$$\begin{bmatrix} b_3 \\ b_4 \end{bmatrix}_C = \begin{bmatrix} s_{31} & s_{32} \\ s_{41} & s_{42} \end{bmatrix}_C \cdot \begin{bmatrix} a_1 \\ a_2 \end{bmatrix}_C \tag{4-3}$$

$$\begin{bmatrix} a_1 \\ a_2 \end{bmatrix}_C = \begin{bmatrix} s_{31} & s_{32} \\ s_{41} & s_{42} \end{bmatrix}_C^{-1} \cdot \begin{bmatrix} b_3 \\ b_4 \end{bmatrix}_C \tag{4-4}$$

$$\begin{bmatrix} b_1 \\ b_2 \end{bmatrix}_C = \begin{bmatrix} s_{11} & s_{12} \\ s_{21} & s_{22} \end{bmatrix}_C \cdot \begin{bmatrix} s_{31} & s_{32} \\ s_{41} & s_{42} \end{bmatrix}_C^{-1} \cdot \begin{bmatrix} b_3 \\ b_4 \end{bmatrix}_C \tag{4-5}$$

$$\begin{bmatrix} b_1 \\ b_2 \end{bmatrix}_D = \begin{bmatrix} s_{11} & s_{12} \\ s_{21} & s_{22} \end{bmatrix}_D \cdot \begin{bmatrix} a_1 \\ a_2 \end{bmatrix}_D \tag{4-6}$$

$$\begin{bmatrix} \hat{b}_1 & \tilde{b}_1 \\ \hat{b}_2 & \tilde{b}_2 \end{bmatrix}_D = \begin{bmatrix} s_{11} & s_{12} \\ s_{21} & s_{22} \end{bmatrix}_D \begin{bmatrix} \hat{a}_1 & \tilde{a}_1 \\ \hat{a}_2 & \tilde{a}_2 \end{bmatrix}_D$$

(4-7)

$$\begin{bmatrix} s_{11} & s_{12} \\ s_{21} & s_{22} \end{bmatrix}_D = \begin{bmatrix} \hat{b}_1 & \tilde{b}_1 \\ \hat{b}_2 & \tilde{b}_2 \end{bmatrix}_D \begin{bmatrix} \hat{a}_1 & \tilde{a}_1 \\ \hat{a}_2 & \tilde{a}_2 \end{bmatrix}_D^{-1}$$

(4-8)

The subscript C refers to the coupler and the subscript D refers to the DUT. The scattering matrix can then be found [Weber, 2001] without the need for the conventional matched terminations by using the equations (4-6) – (4-8). We can see that equation (4-7) is essentially equation (4-6) with two different sets of the vectors "a" and "b". The first set is denoted by "^" and the second set by "~". By equation (4-7), we assume that the perturbation between two measurement sets is small enough that the same scattering matrix can be used. Finally the scattering matrix is found using equation (4-8), assuming the measurement sets are linearly independent so the inverse matrix exists.

The step sizes on the nine points are large enough to allow the difference algorithm to work but not so large as to take the device out of the local region of maximum power.

4.2 Multi-Harmonic Load Pull Measurement

A setup using the multi-harmonic load pull in Figure 4-2 is used here instead of the conventional 50Ω terminations as used in small signal scattering parameter measurement. The setup is similar to that of the large signal load pull measurement case. Two dual directional couplers are also used in the setup but the high speed sampling oscilloscope is used here measuring voltage waveforms at ports "3", "4", "7" and "8" instead of the network analyzer measuring S21, the forward transfer characteristic between port "0" and ports "3", "4", "7" and "8". First, the fundamental source and load tuners are tuned to find the optimum source and load impedance. At the optimum source and load terminations, we perturbed the second harmonic load impedance by a tuning the load tuner at the second harmonic frequency tangentially in the load gamma plane.

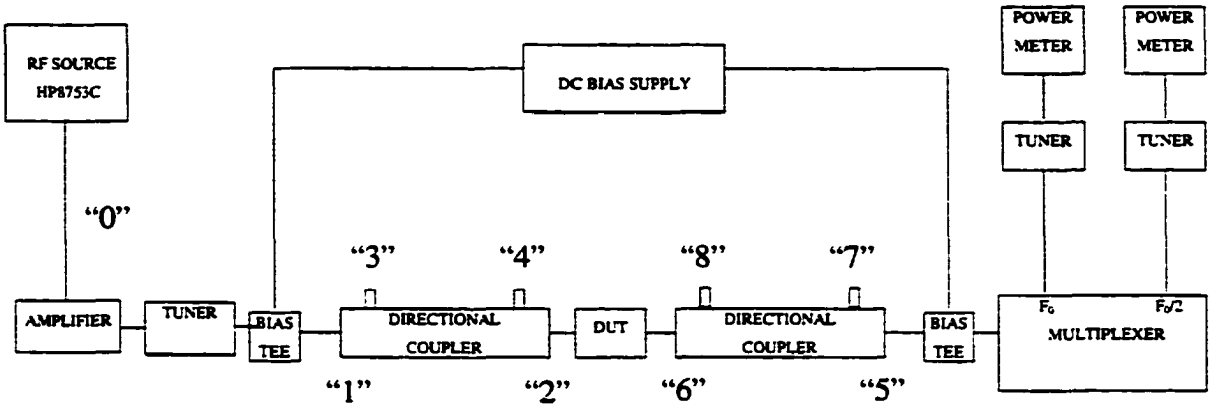

Figure 4-2 Setup for measuring conversion matrix

Considering the voltage waveform measurement data obtained from the sampling oscilloscope, the voltage waveform measured at ports "3", "4", "7" and "8" are actually power wave "b" waveforms at ports "3", "4", "7" and "8" respectively. The calibration using the coupler characteristic in equations 1....8 is applied to get the power waves "a" and "b" at the fixture plane. De-embedding is applied afterward to obtain the power waves "a" and "b" at the device plane. Using fast Fourier transform (FFT) in Matlab™, the spectral component (frequency domain) of both power waves "a" and "b" at the device plane are obtained in the form of magnitude and phase at the fundamental frequency and the harmonic frequencies. These spectral components can then be used to compute the conversion matrix. The large signal scattering parameters can also be computed here but only the spectral components at the fundamental frequency are needed.

5. PROCEDURE, SETUP AND RESULT

5.1 Setup Harmonic Source/Load Pull System to Characterize Microwave Devices

5.1.1 Test and Verify the Functionality of the Fixture

Two fixtures were tested and their functionality verified here. One fixture is for a 1W bipolar part 23A005 from GHz Technology. The other fixture is for a PHEMT part. Both fixtures were tested and their functionality verified at frequencies up to 6 GHz. The fixture of the bipolar part has the active bias controller for the device built in. The circuits are given below in Figure 5-1. For the PHEMT part, the bias is fed through bias tees.

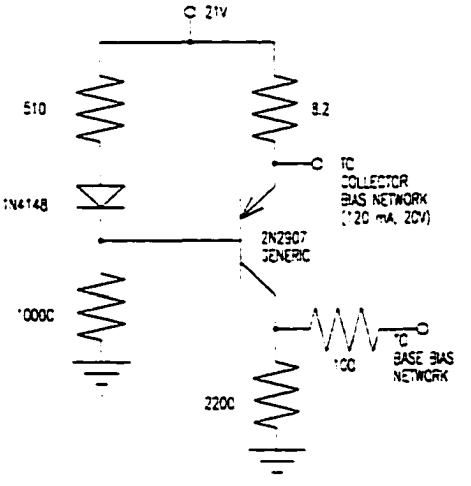

Figure 5-1 Basic schematic of a bias controller of the bipolar part

5.1.2 Characterize the Fixture

The fixture was characterized by recording the scattering parameters for both the first half and the second half of the fixture. Later the scattering parameter file for the first half of the fixture was embedded with the source tuner file and the scattering parameter file for the second half of the fixture was embedded with the load tuner file. These embedded files can then be used with the program written to control the tuners to do source-pull or load-pull.

5.1.3 Write a Program to Deembed the Device

Using the fixture files, one can measure the scattering parameters with the reference plane set at the edge of the fixture and de-embed these scattering parameters to get the scattering parameters at the device plane. The program transforms scattering matrices into T-matrices (cascaded scattering matrices) and uses matrix algebra to get the scattering matrix of the device

5.1.4 Test the 1st 2nd and 3rd Harmonics

In order to determine the variables in a conversion matrix, individual frequency reflection coefficients need to be varied. We initially attempted to do this with a single tuner and varying the tuner position to give a constant fundamental impedance, a circular (or three point) impedance at a given harmonic frequency, and a constant impedance at the remainder of the harmonic frequencies. This should still be possible but in the interest of time, a diplexer was fabricated and used to separate the impedances versus frequency. One tuner was used on the fundamental port of the diplexer and the second tuner was used on either the second or the third harmonic port of the diplexer. The third or second harmonic port was terminated in a 50Ω load. An alternative to this would be to terminate the alternate harmonic signal in some fixed reactance that can easily be done with a sliding short on that port. That would be a procedure for further investigation and might lead to better harmonic data. The diplexer was a cascaded complementary filter [Weber, 2001]. The basic schematic of it is given in Figure 5-2.

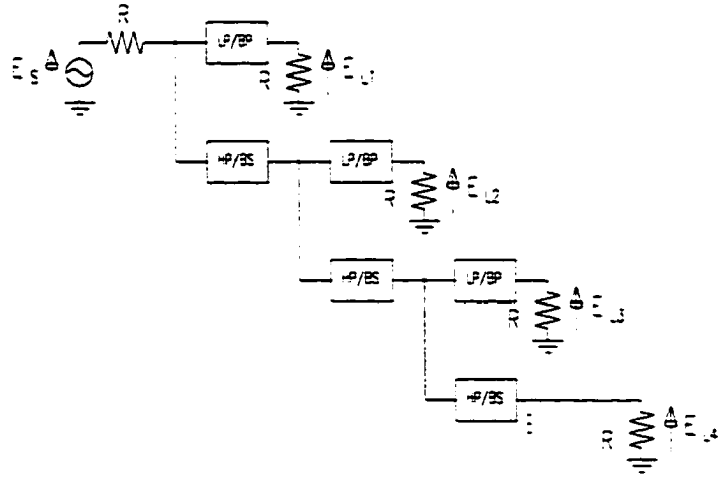

Figure 5-2 Basic schematic of a diplexer

The last load on the right terminates all harmonic signals except the 1st, 2nd, and 3rd. Tests on the1st, 2nd and 3rd harmonic signals using the MRF901 part and the fixture are performed. . The MRF901 part is about a 0.1

watt part. The plots, in Figure 5-3, show the second and third harmonic effect to the output at fundamental. Probe #1 of each tuner is set at 100 and the carriage position is incrementally increased to get a complete circle (one half wavelength).

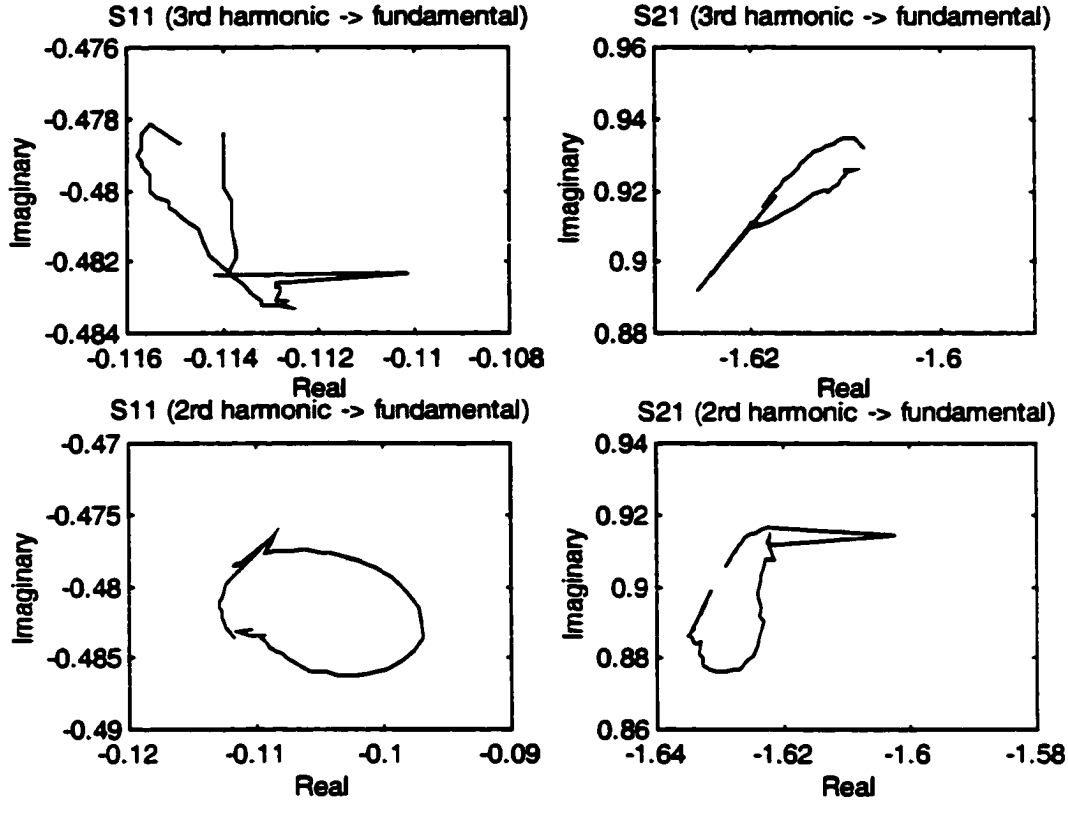

Figure 5-3 Second and third harmonic effects on fundamental load gamma

5.2 Effect of Harmonic Load Pull on a 1W Bipolar Part

The goal of this investigation is to do nonlinear characterization of a 1W bipolar part 23A005 at large signal drive. The bipolar part was biased at 20 volts Vce and 100 mA Ic. The part was excited at 1 GHz and was matched on the input and output at the fundamental frequency 1 GHz to get the output power of 1W. Using the harmonic load pull technique, the load terminations at the second and third harmonic signals (2 and 3 GHz) are tuned as shown in Figure 5-4.

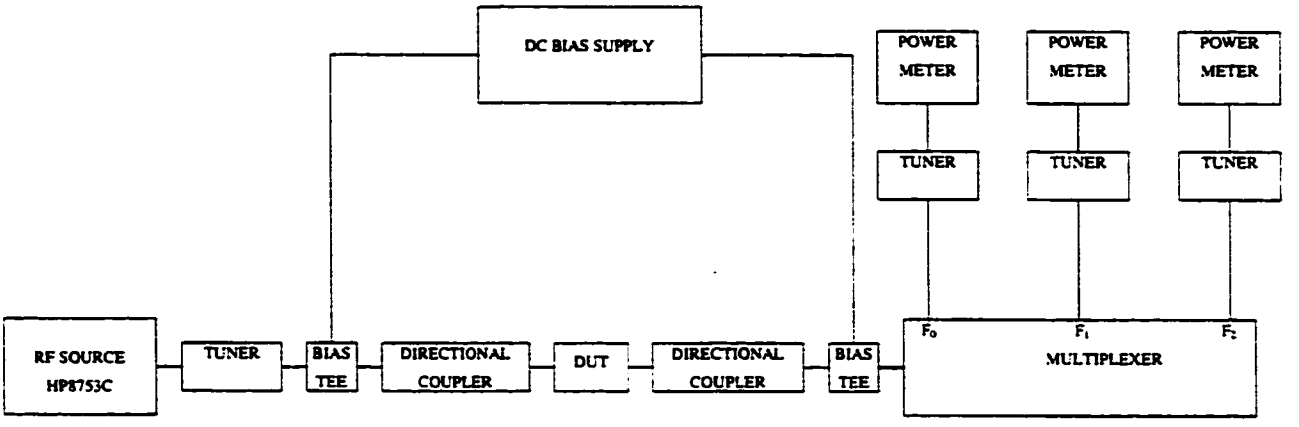

Figure 5-4 Load pull measurement setup

The result is surprising that the second and third harmonic load tuning had little effect on the output power and thus efficiency. The output power varied less than 1% as we tuned the bipolar part. The device package may limit the harmonic effects. We expect to investigate this effect further using some other devices such as PHEMTs.

5.3 Effect of Half Frequency Instability on a 1W Bipolar Part

The results in this section are based on [Weber, 2000].

5.3.1 Measurement Setup

This part of the investigation is to determine a characterization method for determining 1/2 frequency characteristics of a 1W bipolar part 23A005. The setup is shown in Figure 5-5. The bipolar part was biased at 20 volts Vce and 100 mA Ic. The part was excited at 1 GHz from small signal, to full power, and with overdrive. The part had a collector current regulator on it. Full power as used here is sufficient drive to reach nearly fifty percent efficiency but not so much drive that base emitter rectification causes the regulator to lose control of the collector current. Over drive was considered to be the point where the regulator lost control of the collector current and base emitter rectification caused more base current to be generated than was necessary to give 100 mA collector current.

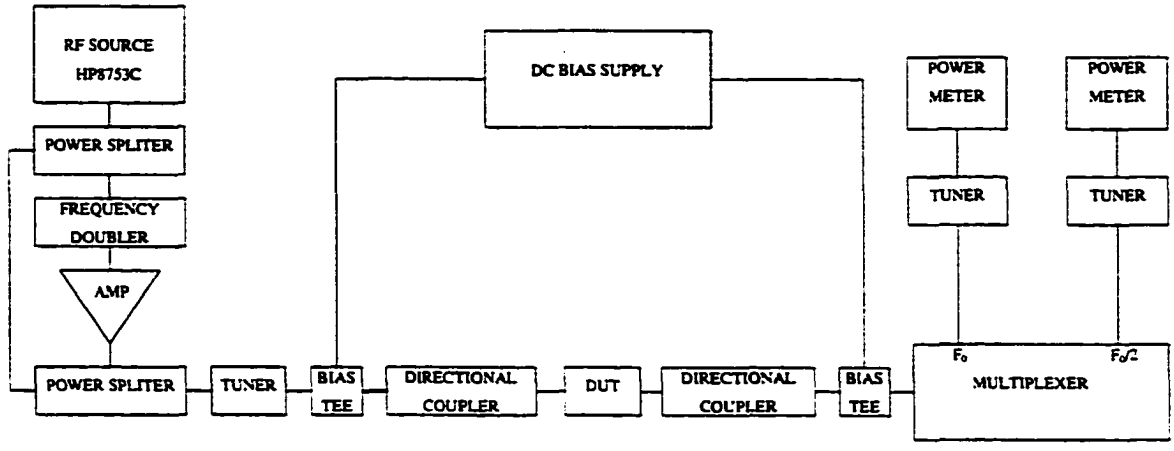

Figure 5-5 Half frequency test setup

With the pump signal at 1 GHz, we measured the part for small signal scattering parameters at 500 MHz while the part was delivering various powers at 1 GHz. The small signal voltage at 500 MHz was at least 20 dB down from the 1 GHz signal. The mixing product, which is 1.5 GHz signal under these conditions was about ten to 20 dB below the 500 MHz signal and was considered small enough to not affect the measurements. When the parts oscillate at 500 MHz, the 1.5 GHz signal would affect the measurements but we were interested in the small signal 500 MHz behavior in order to prevent (1/2 frequency) 500 MHz oscillation.

5.3.2 Large Signal Scattering Parameters

The scattering parameters for the 1 watt part (with fixture included) from full power down to small signal are given in Table 5-1. The input drive at 1 GHz from the network analyzer was varied over a 12 dB range. At each input level, the perturbation of the load reflection coefficient is done in two directions, tangential direction and radial direction. Notice that at the small signal level, the scattering parameters are the same in the tangential and the orthogonal direction. As the part comes closer into saturation, several significant things happen. The input impedance changes slightly. However, notice that the reverse isolation goes down significantly and the phase angle of S12 changes depending on whether the perturbation is tangential or radial. This is the largest single variation and since S12 is very important in the stability equation, the stability parameters are expected to change significantly. The output reflection coefficient also has a larger magnitude and there is a slight change in the angle of S22. The power gain and power delivered are shown in the next data. The data is grouped by power

level. For each power level, there were nine different load used. It is readily seen that the load variations were small to keep the part in a local region of linear operation.

Table 5-1 Large signal scattering parameters of the bipolar part

Input Level	Perturbation Direction	S11		S21		S12		S22	
		Mag	Ang(deg)	Mag	Ang(deg)	Mag	Ang(deg)	Mag	Ang(deg)
-12dB	Tangential	0.95	166	1.71	38	0.02	53	0.46	-137
-12dB	Radial	0.94	166	1.78	37	0.03	47	0.40	-134
-9dB	Tangential	0.94	167	1.58	38	0.03	15	0.54	-136
-9dB	Radial	0.94	166	1.70	36	0.03	35	0.43	-129
-6dB	Tangential	0.95	170	1.22	38	0.03	-63	0.69	-133
-6dB	Radial	0.91	169	1.38	31	0.06	-6	0.56	-116
-3dB	Tangential	0.95	175	0.95	37	0.07	-68	0.75	-129
-3dB	Radial	0.90	173	1.03	29	0.09	-12	0.68	-114
0dB	Tangential	0.96	179	0.83	37	0.11	-72	0.70	-129
0dB	Radial	0.91	177	0.83	30	0.10	-14	0.72	-118

What is most interesting is the change in stability. The stability parameters as a function of drive and load change are shown in Table 5-2. The value of a series resistor on the input of the part necessary to stabilize the part is also shown. It demonstrates that the part becomes increasingly more unstable as it is driven harder.

Table 5-2 Stability factors on the bipolar part

Input Level	Perturbation Direction	K	L	M	RS1
-12 dBm	Tangential	0.95	1.00	0.97	0.06
	Radial	0.80	0.98	0.89	0.29
-9 dBm	Tangential	0.52	0.96	0.81	0.82
	Radial	0.64	0.96	0.81	0.63
-6 dBm	Tangential	0.30	0.94	0.71	1.45
	Radial	0.37	0.90	0.73	1.84
-3 dBm	Tangential	0.16	0.88	0.52	3.46
	Radial	0.17	0.85	0.67	3.54
0 dBm	Tangential	0.20	0.85	0.36	3.85
	Radial	0.06	0.84	0.65	4.19

The three stability parameters are K, L, and M. The criterion is that these parameters need to be greater than one for unconditional stability. K is the inverse of the Linville stability factor [Linville, 1961][Rollet, 1962] and is only a necessary condition. L is a symmetrical necessary and sufficient parameter Weber [Weber, 1987][Weber, 1990] has used for several years. M [Edwards, 1992] is the mu or M stability parameter that is

also necessary and sufficient and used in many CAD programs. Notice that at low drive at 1 GHz, the part is almost stable. The stability suffers greatly as the input drive level increases. RS1 is the series resistance necessary to stabilize the device. The gain would go down considerably with that much resistance used in series with the low input impedance of into the device.

5.3.3 Half Frequency Stability.

While the second harmonic measurements might need more investigation, the 1/2 frequency (fundamental to the network analyzer) measurements don't have that difficulty. At 500 MHz, the small signal scattering parameters measured directly on the device are shown in Table 5-3 and the following KLM stability values.are shown in Table 5-4.

Table 5-3 Scattering parameters of a bipolar part at 500 MHz small signal

Frequency (0.5 GHz)							
S11		S21		S12		S22	
Mag	Ang(deg)	Mag	Ang(deg)	Mag	Ang(deg)	Mag	Ang(deg)
0.91	174	4.04	75	0.02	26	0.28	-110

Table 5-4 Stability of a bipolar part at 500 MHz small signal

Frequency (0.5 GHz)		
K	L	M
0.85	0.98	0.90

At 500 MHz, the small signal scattering parameters measured while the part was being excited at small signal at 1 GHz for various load position at 500 MHz are shown in Table 5-5. Although there are some variations as the load is pulled at 500 MHz while the part is operating at 1 GHz, the parameters are close to the small signal values. The variation is believed to be due to the 1 GHz signal leaking back into network analyzer from the output of the doubler. The stability values for these parameters are shown in Table 5-6.

Table 5-5 Scattering parameters at 0.5 GHz with the part excited small signal at 1 GHz

Frequency (0.5 GHz)							
S11		S21		S12		S22	
Mag	Ang(deg)	Mag	Ang(deg)	Mag	Ang(deg)	Mag	Ang(deg)
0.87	177	3.21	54	0.01	-23	0.43	-116
0.88	175	3.50	53	0.02	0	0.49	-100
0.87	175	3.73	55	0.02	-11	0.45	-88
0.90	174	3.90	59	0.02	27	0.35	-80
0.86	174	3.92	65	0.03	5	0.23	-92
0.90	173	3.78	69	0.02	31	0.26	-117
0.92	174	3.54	71	0.02	10	0.35	-116
0.92	174	3.36	71	0.01	20	0.40	-108
0.91	174	3.12	69	0.02	27	0.42	-92
0.90	175	3.23	62	0.03	18	0.23	-87

Table 5-6 Stability at 0.5 GHz with the part excited at 1 GHz small signal

Frequency (0.5 GHz)		
K	L	M
3.26	1.13	1.57
0.71	0.95	0.87
1.01	1.00	1.00
0.65	0.94	0.79
0.85	0.96	0.89
0.87	0.98	0.91
0.98	1.00	0.99
1.02	1.00	1.01
0.83	0.98	0.92
0.73	0.95	0.80

On the basis of the stability parameters (comparing to the small signal values) the first, third, and seventh measurements are likely the least accurate. Again, it is believed that the accuracy will be improved with isolation on the a port of the network analyzer (not the a port of the DUT). When the part is putting out 1 watt, the 500 MHz scattering parameters are shown in Table 5-7. The forward gain is reduced as expected and there are some variations in the parameters. The stability factors for these scattering parameters are shown in Table 5-8.

Table 5-7 Scattering parameters at 0.5 GHz with the part excited large signal at 1 GHz

Frequency (0.5 GHz)							
S11		S21		S12		S22	
Mag	Ang(deg)	Mag	Ang(deg)	Mag	Ang(deg)	Mag	Ang(deg)
0.63	-158	1.79	21	0.08	-53	0.88	-104
0.61	-159	2.01	24	0.10	-45	0.94	-90
0.58	-164	2.09	31	0.13	-25	0.82	-79
0.60	-169	2.32	39	0.12	-6	0.66	-60
0.69	-174	2.26	55	0.08	23	0.25	-62
0.77	-167	1.63	72	0.05	-46	0.56	-130
0.79	-164	1.12	67	0.08	-57	0.81	-105
0.77	-160	0.85	50	0.11	-30	0.88	-81
0.78	-157	0.92	33	0.14	-14	0.64	-64
0.69	-158	1.36	29	0.02	1	0.39	-132

Table 5-8 Stability at 0.5 GHz with the part excited large signal at 1 GHz

Frequency (0.5 GHz)		
K	L	M
0.879	0.964	0.963
0.656	0.858	0.869
0.706	0.839	0.849
0.823	0.898	0.887
1.325	1.119	1.254
1.564	1.084	1.163
0.670	0.943	0.913
0.663	0.938	0.915
1.219	1.057	1.133
7.684	1.379	2.128

Again, the variation is likely due to the leakage of the 1 GHz signal at the drive port of the network analyzer. However, it is significant that the stability factors are about the same for the 1 Watt drive level as for small signal. When the part is over driven, the 500 MHz scattering parameters are shown in Table 5-9. It is quite significant that now S11 has a magnitude greater than one. There is some variation with respect to the other parameters (quite a bit on S21 and S22). This would be expected since the collector voltage (1 GHz plus small signal 500 MHz) is limited by the device. These data indicate that one could expect 500 MHz small signal oscillation unless that signal path is damped. The 500 MHz small signal oscillation current will mix with the fundamental and cause 1.5 GHz spurious. Often the base (and often the collector) bias lines have a low impedance to the 500 MHz signal so that the signal is not readily seen at the output. However, the current exist

in the device and generate the 1-1/2 signal. Note the angle of S11. As expected from these scattering parameters, the stability factors would vary as a function of the 500 MHz load on the collector (although a significant amount of this variation is likely due to network analyzer error due to the 1 GHz signal leakage).

Table 5-9 Scattering parameters at 0.5 GHz with the part over driven at 1 GHz

Frequency (0.5 GHz)							
S11		S21		S12		S22	
Mag	Ang(deg)	Mag	Ang(deg)	Mag	Ang(deg)	Mag	Ang(deg)
1.33	162	5.21	76	0.30	-25	1.54	-79
1.43	169	5.27	92	0.26	-7	1.25	-49
1.70	177	5.52	106	0.27	29	1.14	-20
1.59	-174	3.87	118	0.15	40	0.30	-22
1.48	-166	2.77	120	0.05	33	0.36	-112
1.28	-160	1.72	107	0.10	-47	0.85	-103
1.10	-162	1.62	80	0.16	-21	0.96	-82
0.98	-160	1.87	63	0.19	-7	0.85	-66
0.84	-169	2.44	52	0.14	20	0.55	-53
1.03	177	3.51	70	0.09	-66	0.85	-116

The stability factors for the over drive case at 500 MHz are shown in Table 5-10. These values indicate a large level of instability at 500 MHz from this over driven condition. (Note: the part is producing 1.4 watts at 1 GHz for these parameters).

Table 5-10 Stability at 0.5 GHz with the part over driven at 1 GHz

Frequency (0.5 GHz)		
K	L	M
-0.61	-4.07	-0.27
-0.56	-3.31	-0.41
-0.87	-4.50	-0.78
-1.36	-1.77	-1.43
-3.83	-0.34	-2.15
-1.26	0.20	-1.12
-0.48	0.24	-0.41
0.02	0.29	0.05
0.27	0.51	0.40
-0.34	0.15	-0.09

5.3.4 Summary

This report presents a characterization method for measuring the 1/2 frequency behavior of a bipolar part. It is not limited to this 1 GHz bipolar part. Similar measurement could be made on other non-linear parts including FETs. These data demonstrate what has been anticipated. The bipolar part is more and more unstable as it is driven with higher and higher levels of input drive. When the input drive is large enough that the base to emitter rectification overcomes the input bias, the part becomes very unstable.

The data taken at 1 GHz and high power operation using the network analyzer in the fundamental mode are quite good. The data taken at 1 GHz using the network analyzer in the second harmonic mode would require further work to increase the accuracy of the data. However, trends in the data can be used to give the circuit designed the additional criteria needed to stabilize high power bipolar amplifiers beyond what is available from small signal parameters. These data are available from measurements and don't require large amounts of computational time.

The data taken at 500 MHz with the network analyzer having significant amounts of the second harmonic (1 GHz) energy feed back into it (not into the sample ports but into the RF out port) is good but it is believed that the accuracy of the data will be much improved with better isolation in that path.

5.4 Effect of the Harmonic Source/Load Pull on PHEMT at 0.5 GHz

5.4.1 PHEMT Measurement Setup

The bias controller, shown in Figure 5-6, is built to provide a good stable bias to the PHEMT part. The voltage on the gate can be adjusted between -1.5 V to 0.5 V using the potentiometer. The voltage on the drain is fixed at 5 V. We use the voltage follower output configuration of the operational amplifier to provide the voltage to the part so that a constant voltage level can be obtained while tuning the part. We get a good constant voltage level but the current level is fluctuating with the tuning and the drive level. Some kind of current controller may be added to the bias controller in the future to eliminate this problem.

The part appears to be operating correctly with a maximum efficiency of 50 % at 0.5 GHz after tuning the fundamental and second harmonic signals on both input and output.

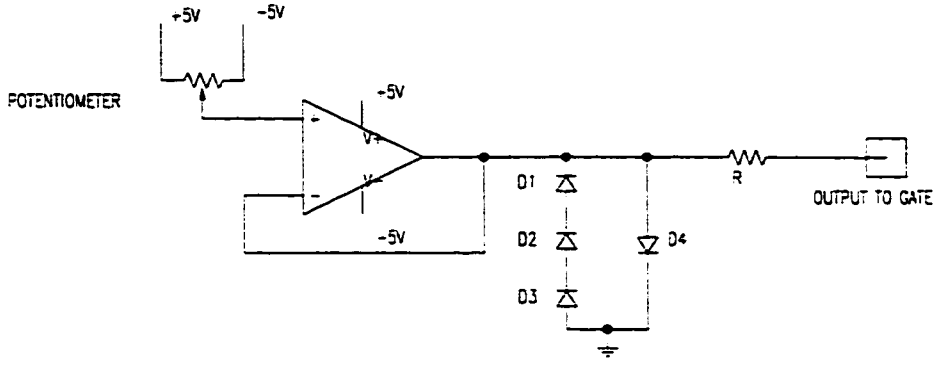

Figure 5-6 Schematic of the bias controller for adjusting gate volage

5.4.2 Output Harmonic Tuning

In order to see the effect of harmonic tuning on the output of the part, the setup, in Figure 5-7, is used. We tune the input and output terminations at both the fundamental frequency and the second harmonic frequency the in order for the device to achieve maximum power. Then we sweep the Maury Tuner MT982E on the second harmonic port of the diplexer on the output from end to end with the big slug set at 0 (like a short) and take measurements. Using the network analyzer with a power setting of 20 dBm (actual output = 16 dBm) at a frequency of 0.5 GHz the following measurements were made as shown in Table 5-11. Three numbers represent the tuner position. The first number is the carriage position, which is the horizontal position of the two slugs along the transmission line. The carriage position is varied in such a way that the load reflection coefficient is varied 360°, a complete circle in the Smith chart plot. The second number represents the position of the big slug and it can be varied from 0 to 5000, with 0 being the position that the big slug is closest to the transmission line and 5000 being the position that the big slug is farthest away from the transmission line. The third number is the position of the small slug and it also can be varied from 0 to 5000. The power measurement is made on the forward and reverse direction of the 20 dB dual directional coupler on the output because this would give a more accurate measurement. The power waves in the forward and reverse direction are measured in dBm. Both of the power waves (in mW) can be found by using the characteristic of the coupler. The real output power (in mW) can then be obtained from the difference of the power waves (in mW) in the forward and reverse direction.

Table 5-11 Effect of output tuning on power output

"Second Harmonic" Tuner Position	Power Measurement		
	Forward (dBm)	Reverse (dBm)	Power(mW)
2000 0 5000	2.55	-3.90	350
4000 0 5000	2.53	-3.94	348
6000 0 5000	2.53	-3.98	349
8000 0 5000	2.53	-3.97	349
10000 0 5000	2.53	-3.95	348
12000 0 5000	2.53	-3.94	348
14000 0 5000	2.53	-3.93	348
16000 0 5000	2.55	-3.91	350
18000 0 5000	2.55	-3.93	350
20000 0 5000	2.53	-3.98	349

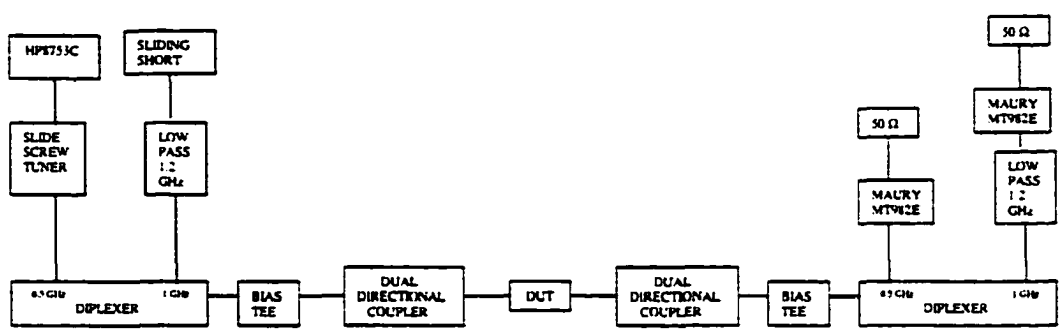

Figure 5-7 Output harmonic tuning setup

5.4.3 Input Harmonic Tuning

To tune the harmonic termination on the input of the part, the setup, in Figure 5-8, is used. We tune the input and output terminations at both the fundamental frequency and the second harmonic frequency the in order for the device to achieve maximum power. Then we sweep the Maury Tuner MT982E on the second harmonic port of the diplexer on the output from end to end with the big slug set at 0 (like a short) and take measurements. Using the network analyzer with a power setting of 20 dBm (actual output = 16 dBm) at a frequency of 0.5 GHz the following measurements were made as shown in Table 5-12. Three numbers represent the tuner position. The first number is the carriage position, which is the horizontal position of the two slugs along the transmission line. The carriage position is varied in such a way that the load reflection coefficient is varied 360°, a complete

circle in the Smith chart plot. The second number represents the position of the big slug and it can be varied from 0 to 5000, with 0 being the position that the big slug is closest to the transmission line and 5000 being the position that the big slug is farthest away from the transmission line. The third number is the position of the small slug and it also can be varied from 0 to 5000. The power measurement is made on the forward and reverse direction of the 20 dB dual directional coupler on the output because this would give a more accurate measurement. The power waves in the forward and reverse direction are measured in dBm. Both of the power waves (in mW) can be found by using the characteristic of the coupler. The real output power (in mW) can then be obtained from the difference of the power waves (in mW) in the forward and reverse direction.

Table 5-12 Effect of input tuning on power output

"Second Harmonic" Tuner Position	Power Measurement		
	Forward (dBm)	Reverse (dBm)	Power (mW)
2000 0 5000	1.85	-5.44	312
4000 0 5000	1.93	-5.38	319
6000 0 5000	1.96	-5.38	322
8000 0 5000	1.93	-5.39	319
10000 0 5000	1.85	-5.42	312
12000 0 5000	1.70	-5.42	300
14000 0 5000	1.55	-5.48	288
16000 0 5000	1.61	-5.58	295
18000 0 5000	1.82	-5.50	311
20000 0 5000	1.93	-5.44	320

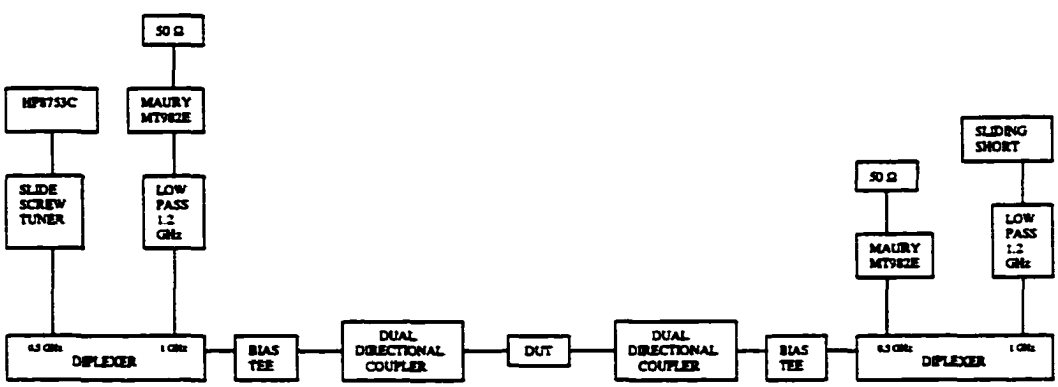

Figure 5-8 Input harmonic tuning setup

5.4.4 Conclusion

The results from tuning the second harmonic terminations on the input and output of the device are as expected. The square law characteristic of the FET supports the idea that the shaping of the voltage waveform especially using the second harmonic tuning on the gate (the harmonic input tuning) would benefit the power output and efficiency of the part. As can see that the power output varies more in the case of the input harmonic tuning than the output harmonic tuning. The nonlinear characterization of this part using the conversion matrix will be investigated next. This should help us to be able to predict the effect of input and output tuning on the performance of the part.

5.5 Large Signal Scattering Parameters of The PHEMT Part at 1 GHz

5.5.1 PHEMT Measurement Setup

The bias controller, shown in Figure 5-6, is built to provide a good stable bias to the PHEMT part. The voltage on the gate can be adjusted between -1.5 V to 0.5 V using the potentiometer. We use the voltage follower output configuration of the operational amplifier to provide the voltage to the part so that a constant voltage level can be obtained while tuning the part. We get a good constant voltage level but the current level is fluctuating with the tuning and the drive level. Some kind of current controller can be added to the bias controller in the future to eliminate this problem. The setup can be seen in Figure 5-9. The fundamental tuners on the input and output are tuned to obtain maximum power output from the nonlinear device at 1 GHz. The relationship between the fundamental frequency and the second harmonic frequency components of the nonlinear device is obtained as the Maury Tuner MT982E at the fundamental frequency on the output is tuned radially and tangentially. The Maury tuner at the second harmonic port of the diplexer on the output is set fixed with both plungers at position 0. The gate voltage is set at –0.41 Vand the drain voltage 5 V. The drain current is measured to be 137 mA. The part appears to be operating correctly with a maximum efficiency of 24 % after the impedances at the fundamental frequency on both input and output are tuned for maximum power output.

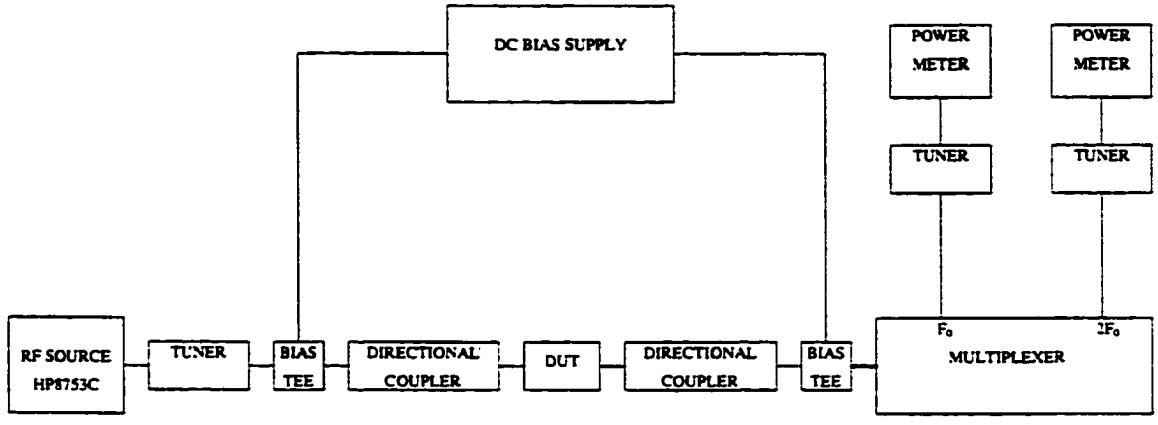

Figure 5-9 Setup for measuring large signal scattering parameters

5.5.2 Large Signal Scattering Parameter Result

The scattering parameters of two PHEMTs are presented here. In the large signal case, the first PHEMT is measured using both the network analyzer and the sampling oscilloscope in order to verify the validity of the waveform measurement using the sampling oscilloscope and the FFT function in MATLAB™. The large signal scattering parameters of the first PHEMT from the measurement using the sampling oscilloscope is designated as $[S]_{PHEMT1\text{-}SO}$, and from the measurement using the sampling oscilloscope is designated as $[S]_{PHEMT1\text{-}NA}$.

$$[S]_{PHEMT1\text{-}SO} = \begin{bmatrix} 0.68\angle 165 & 0.06\angle -9 \\ 4.07\angle 119 & 0.75\angle 153 \end{bmatrix}$$

$$[S]_{PHEMT1\text{-}NA} = \begin{bmatrix} 0.67\angle 163 & 0.06\angle 14 \\ 3.68\angle 118 & 0.73\angle 150 \end{bmatrix}.$$

The measurement is then performed on both PHEMTs in the small signal case and the large signal case. In the small signal case, the PHEMTs are hooked up to just the network analyzer whose termination is 50Ω. The bias, being fed through the internal circuitry of the network analyzer, comes out from both port 1 and port 2 of the network analyzer. In the large signal case, the waveforms are measured using the sampling oscilloscope at the coupler ports. The bias is provided to the devices by means of a pair of bias tees. The results are presented in Table 5-13.

Table 5-13 Small signal and large signal scattering parameters of two PHEMTs

Small signal (Using NA for measurement, 50 ohms) VS. Large signal (load and source pull, coupler deembedding, sampling scope)								
	MAG(S11)	ANG(S11)	MAG(S21)	ANG(S21)	MAG(S12)	ANG(S12)	MAG(S22)	ANG(S22)
small signal PHEMT1 (-10 dBm+NA 50 ohms)	0.71	157	4.00	116	0.05	-19	0.76	144
small signal PHEMT2 (-10 dBm+NA 50 ohms)	0.76	154	4.41	118	0.04	-19	0.76	140
large signal PHEMT1 (20dBm+COUPLER+SAMPLING SCOPE)	0.68	166	4.07	119	0.06	-9	0.75	153
large signal PHEMT2 (20dBm+COUPLER+SAMPLING SCOPE)	0.62	168	3.62	120	0.07	-24	0.61	153

5.5.3 Conclusion

Both results of the first PHEMT using the sampling oscilloscope and using the network analyzer agree. This indicates that our in house MATLAB™ program using FFT algorithm on the waveform measurement from the sampling oscilloscope works as well as the network analyzer in measuring large signal scattering parameters at fundamental frequency. This gives us the confidence of adapting this algorithm in order to compute the conversion matrix in the next section. The resulting large signal scattering parameters from the two measurements are almost identical. Also the small signal scattering parameters, measured when the terminations are 50Ω, are compared with the large signal scattering parameters measured when the terminations are not 50Ω. The results are slightly different which is what we expected since both PHEMTs are operating in the nonlinear region in the large signal case and in the linear region in the small signal case.

5.6 Conversion Matrix of The PHEMT Part at 1 GHz

5.6.1 PHEMT Measurement Setup

The setup is the same as that in the large signal scattering parameter setup in the previous section.

5.6.2 Conversion Matrix Result

The conversion matrices are presented here. $[S]_{PHEMT1\text{-}M1}$ is the conversion matrix of the first PHEMT obtained by the perturbation as the fundamental load is varied in the tangential and radial directions. $[S]_{PHEMT1\text{-}C1}$ is the conversion matrix of the first PHEMT obtained by the perturbation as the load at the second harmonic frequency is varied along the circle (as a sliding short). $[S]_{PHEMT2\text{-}M1\text{-}1}$ is the conversion matrix of the second PHEMT obtained by the perturbation as the fundamental load is varied in the tangential and radial directions. $[S]_{PHEMT2\text{-}M1\text{-}2}$ is just a repeat measurement of $[S]_{PHEMT2\text{-}M1\text{-}1}$ to see if the conversion matrix changes when measurement is taken from the identical setup. $[S]_{PHEMT2\text{-}M2\text{-}1}$ is the conversion matrix of the second PHEMT

obtained by the perturbation as the fundamental load is varied in the tangential and radial directions when the fundamental load is not in the same local region (the load reflection coefficient is rotated by about 40 degrees). $[S]_{PHEMT2\text{-}M2\text{-}2}$ is just a repeat measurement of $[S]_{PHEMT2\text{-}M2\text{-}1}$ to see if the conversion matrix changes when measurement is taken from the identical setup.

$$[S]_{PHEMT1\text{-}M1} = \begin{bmatrix} 0.70\angle 170 & 6.61\angle 96 & 0.05\angle -15 & 2.36\angle -22 \\ 0.04\angle -12 & 3.76\angle -94 & 0.01\angle -117 & 0.96\angle 136 \\ 4.13\angle 120 & 10.62\angle 0 & 0.81\angle 153 & 2.95\angle -81 \\ 0.07\angle -161 & 5.74\angle 54 & 0.06\angle -178 & 2.11\angle -58 \end{bmatrix}$$

$$[S]_{PHEMT1\text{-}C1} = \begin{bmatrix} 0.78\angle 66 & 6.28\angle 36 & 0.76\angle -70 & 1.59\angle 24 \\ 0.06\angle -113 & 1.02\angle -169 & 0.01\angle 169 & 0.12\angle -90 \\ 1.02\angle 90 & 10.20\angle 11 & 2.50\angle -163 & 2.08\angle 26 \\ 0.21\angle -7 & 1.95\angle 37 & 0.21\angle -97 & 0.54\angle 126 \end{bmatrix}$$

$$[S]_{PHEMT2\text{-}M1\text{-}1} = \begin{bmatrix} 0.63\angle 166 & 0.19\angle 166 & 0.10\angle 19 & 1.45\angle -20 \\ 0.05\angle -96 & 0.72\angle -176 & 0.01\angle -164 & 0.61\angle 8 \\ 3.49\angle 119 & 4.65\angle 30 & 0.24\angle -145 & 12.33\angle -130 \\ 0.05\angle -70 & 0.17\angle -143 & 0.08\angle -65 & 0.36\angle 28 \end{bmatrix}$$

$$[S]_{PHEMT2\text{-}M1\text{-}2} = \begin{bmatrix} 0.54\angle 166 & 2.97\angle 177 & 0.20\angle -8 & 1.35\angle -68 \\ 0.06\angle -87 & 0.79\angle -164 & 0.03\angle -95 & 0.02\angle -149 \\ 3.59\angle 122 & 4.99\angle -74 & 0.83\angle 178 & 10.56\angle 144 \\ 0.05\angle -41 & 0.96\angle -119 & 0.11\angle -48 & 0.36\angle -116 \end{bmatrix}$$

$$[S]_{PHEMT2\text{-}M2\text{-}1} = \begin{bmatrix} 0.54\angle 170 & 2.53\angle 179 & 0.17\angle -38 & 1.24\angle -165 \\ 0.06\angle -173 & 1.46\angle -52 & 0.08\angle 126 & 1.12\angle 15 \\ 3.43\angle 131 & 16.77\angle 60 & 1.20\angle -176 & 7.10\angle 129 \\ 0.03\angle -100 & 0.90\angle -20 & 0.07\angle -69 & 0.12\angle 37 \end{bmatrix}$$

$$[S]_{PHEMT2\text{-}M2\text{-}2} = \begin{bmatrix} 0.72\angle 176 & 3.32\angle 52 & 0.14\angle -148 & 2.58\angle 94 \\ 0.09\angle -60 & 2.09\angle -180 & 0.07\angle -67 & 0.40\angle -151 \\ 3.99\angle 124 & 8.27\angle -72 & 1.86\angle 151 & 24.03\angle 67 \\ 0.04\angle -25 & 0.94.\angle -61 & 0.11\angle -22 & 1.61\angle -69 \end{bmatrix}$$

5.6.3 Conclusion

The conversion matrices $[S]_{PHEMT1\text{-}M1}$, $[S]_{PHEMT1\text{-}C1}$, $[S]_{PHEMT2\text{-}M1\text{-}1}$ and $[S]_{PHEMT2\text{-}M1\text{-}2}$ are obtained while the load at fundamental is in the same local region. The results differ very much even between the repeated measurements $[S]_{PHEMT2\text{-}M1\text{-}1}$ and $[S]_{PHEMT2\text{-}M1\text{-}2}$. This indicates the sensitivity of the conversion matrix model on the operation point. Note that the result $[S]_{PHEMT1\text{-}C1}$ obtained from varying the load at the second harmonic frequency is subject to error since the spectral components of the power waves "a" and "b" (not included in this paper) are almost identical between measurement at the points along the circle. This demonstrates the disadvantage of using the perturbation method to characterize the nonlinear device in the local region. One interesting observation is that the effect of the second harmonic signal on the fundamental signal is greater then the effect of the fundamental signal on the second harmonic signal in the same local region. This observation really supports the idea of doing the harmonic load and source pull to gain more performance at the fundamental frequency as can be seen in Table 5-11and Table 5-12. Since the conversion matrix is a large signal – small signal characterization, the robustness problem will play a significant role in this characterization. Another interesting observation is that $s_{11,11}$ and $s_{21,11}$, see definition in equation (3-11), don't change very much between measurements even when the fundamental load is not in the same local region.

The usefulness of the conversion matrix in characterizing nonlinear microwave devices operating at a large signal input level is limited as seen in the results. The conversion matrix is an attempt to use linear method to characterize nonlinear devices. The results indicate that the conversion matrix fails to characterize the nonlinear device successfully as the cross-frequency terms and the second harmonic terms in the conversion matrix change drastically between measurements.

The conclusion can be made from this research that in order to fully characterize a nonlinear microwave device (including the relationship between the harmonic frequencies and the fundamental frequency), nonlinear methods should be deployed rather than an attempt to linearize the nonlinear device in the local region. This is due to the fact that the nonlinear behavior is not linear even when considered in a small local region (for the perturbation algorithm to work).

6. APPENDIX

6.1 Characteristic of 1-2-3 GHz Diplexer

S11 and S21 between the input port and the output ports (fundamental, second and third harmonic) are shown in Figure 6-1, Figure 6-2 and Figure 6-3. S11 is the input reflection coefficient so it indicates the matching performance of the diplexer on the input port. S21 is the forward transmission coefficient so it indicates the filtering performance of the diplexer in distinguishing between the fundamental signal , the second harmonic signal and the third harmonic signal.

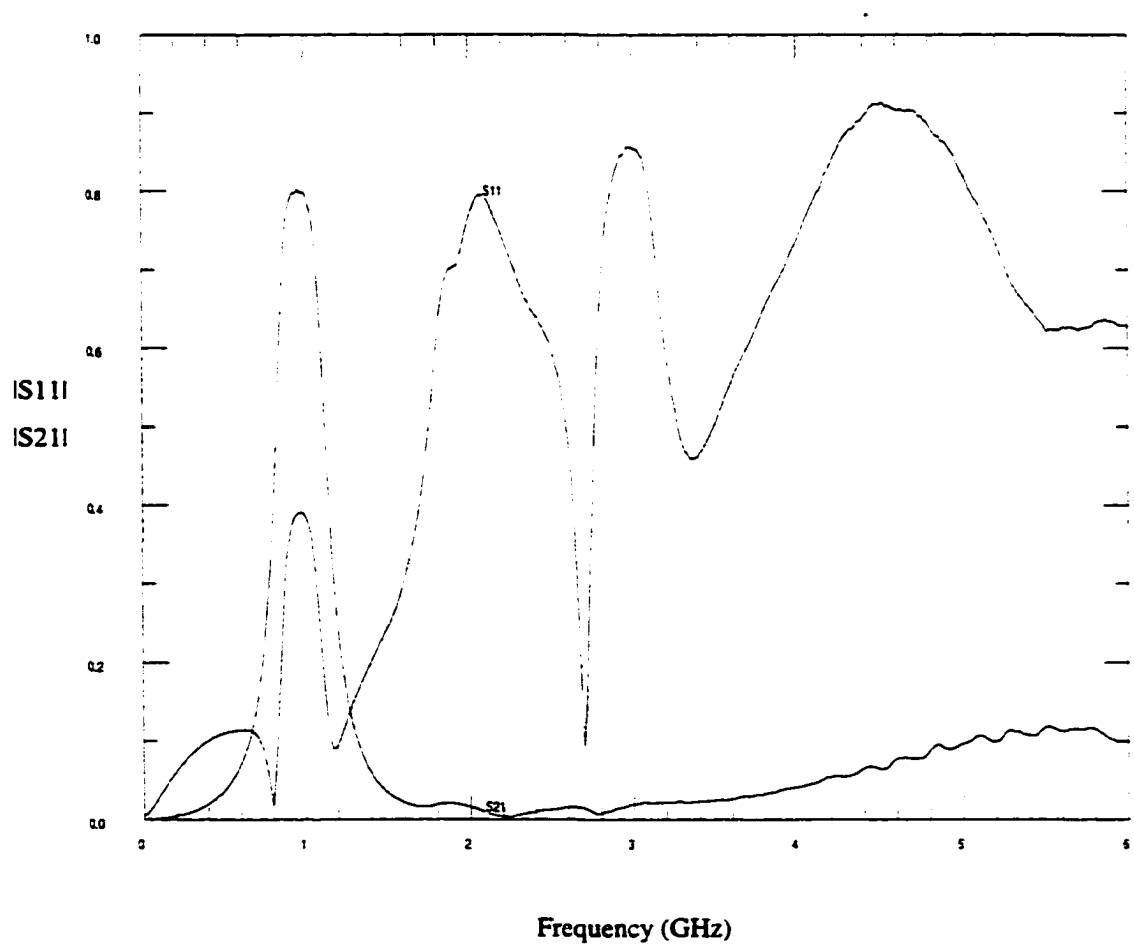

Figure 6-1 Characteristic between input port and fundamental port

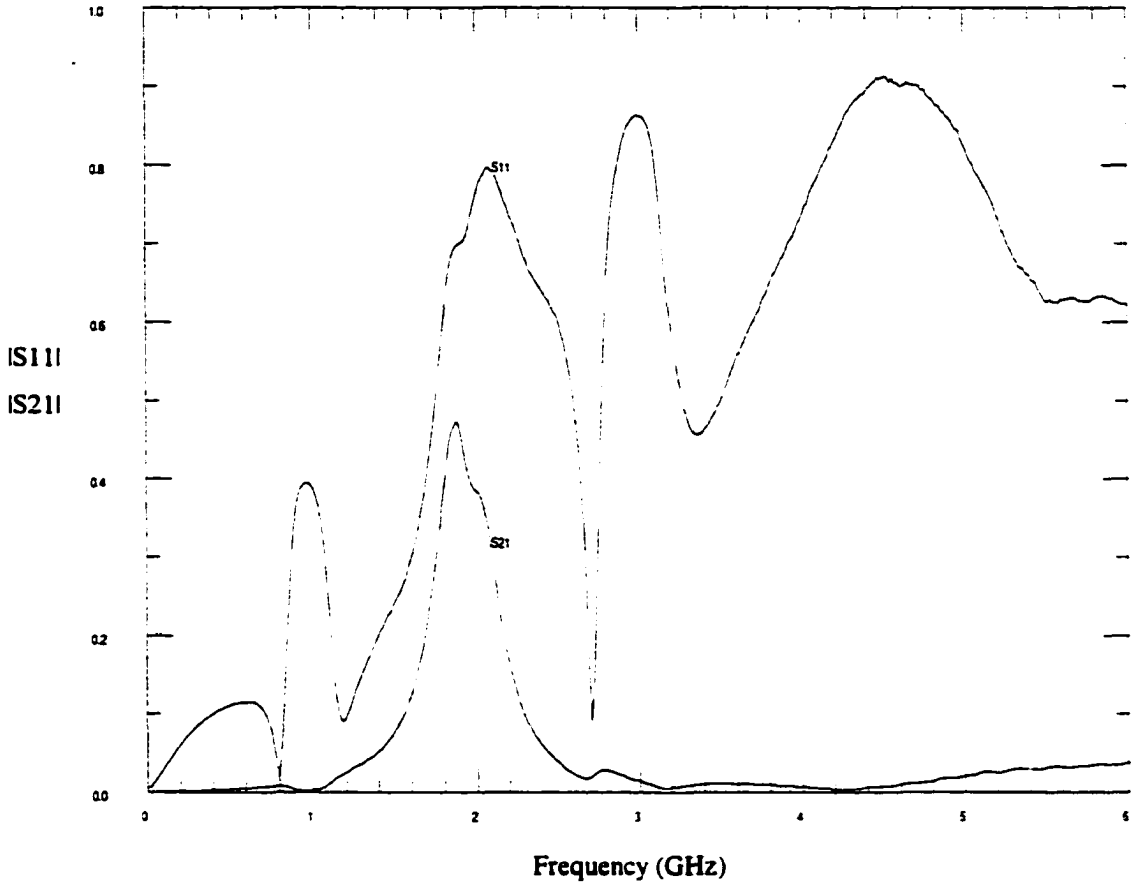

Figure 6-2 Characteristic between the input port and the second harmonic port

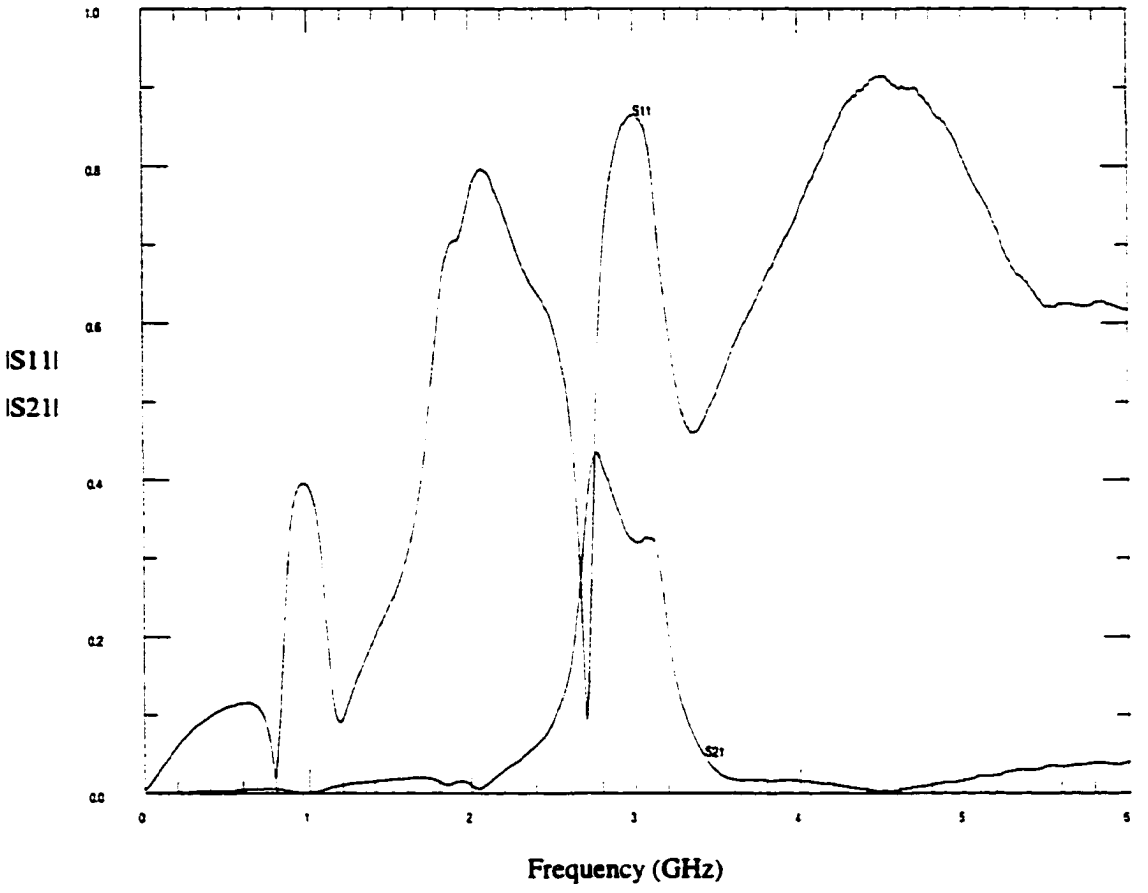

Figure 6-3 Characteristic between the input port and the third harmonic port

6.2 Characteristic of 0.5-1 GHz Diplexer

We used a ten-pole, 707 MHz filter to accomplish simultaneous measurements at 500 MHz and 1 GHz. The response of this diplexing pair is shown in Figure 6-4 and Figure 6-5. S11 was measured on the input port and it indicates the matching characteristic of the diplexer. LP (low pass response) and HP (high pass response) are S21 measured between the input port and the output ports (0.5 GHz and 1 GHz, respectively).

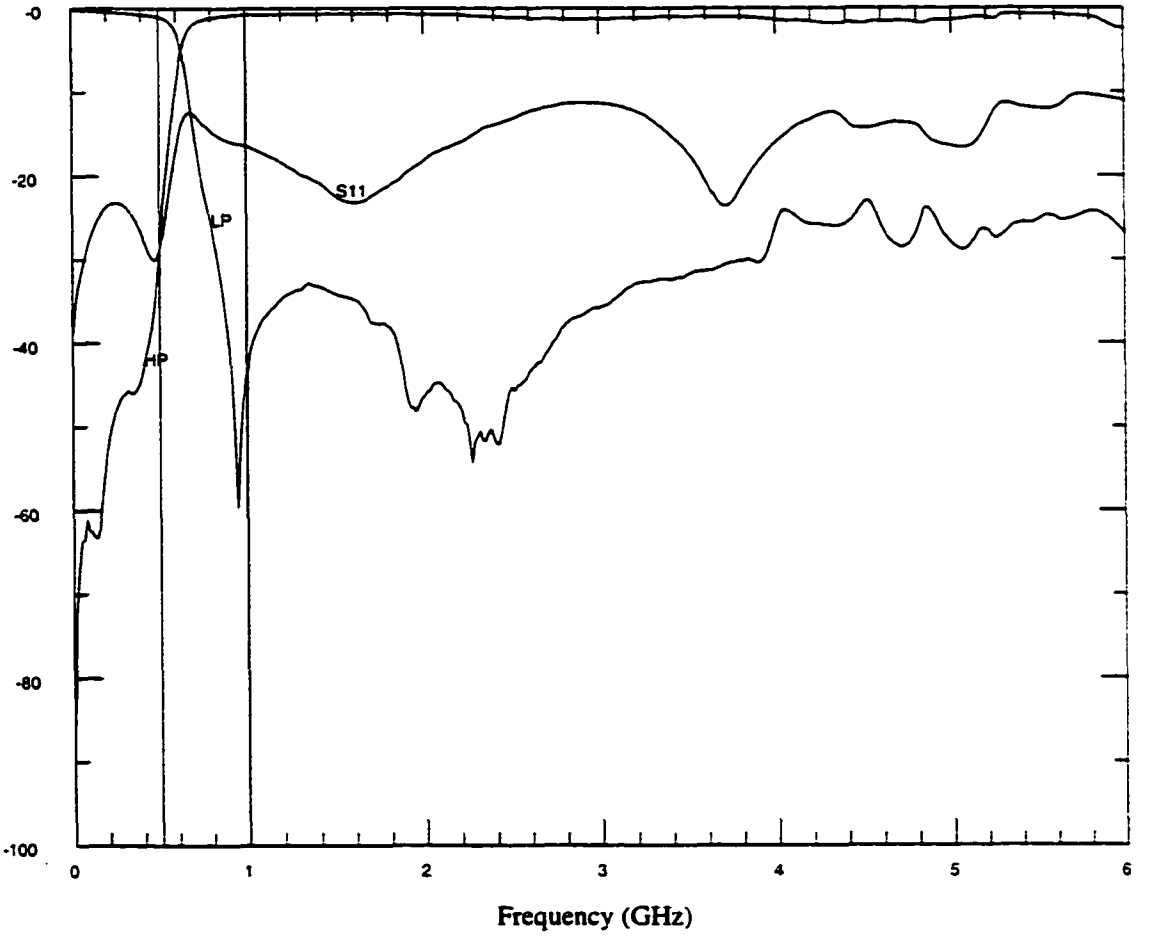

Figure 6-4 Response of the diplexer filter

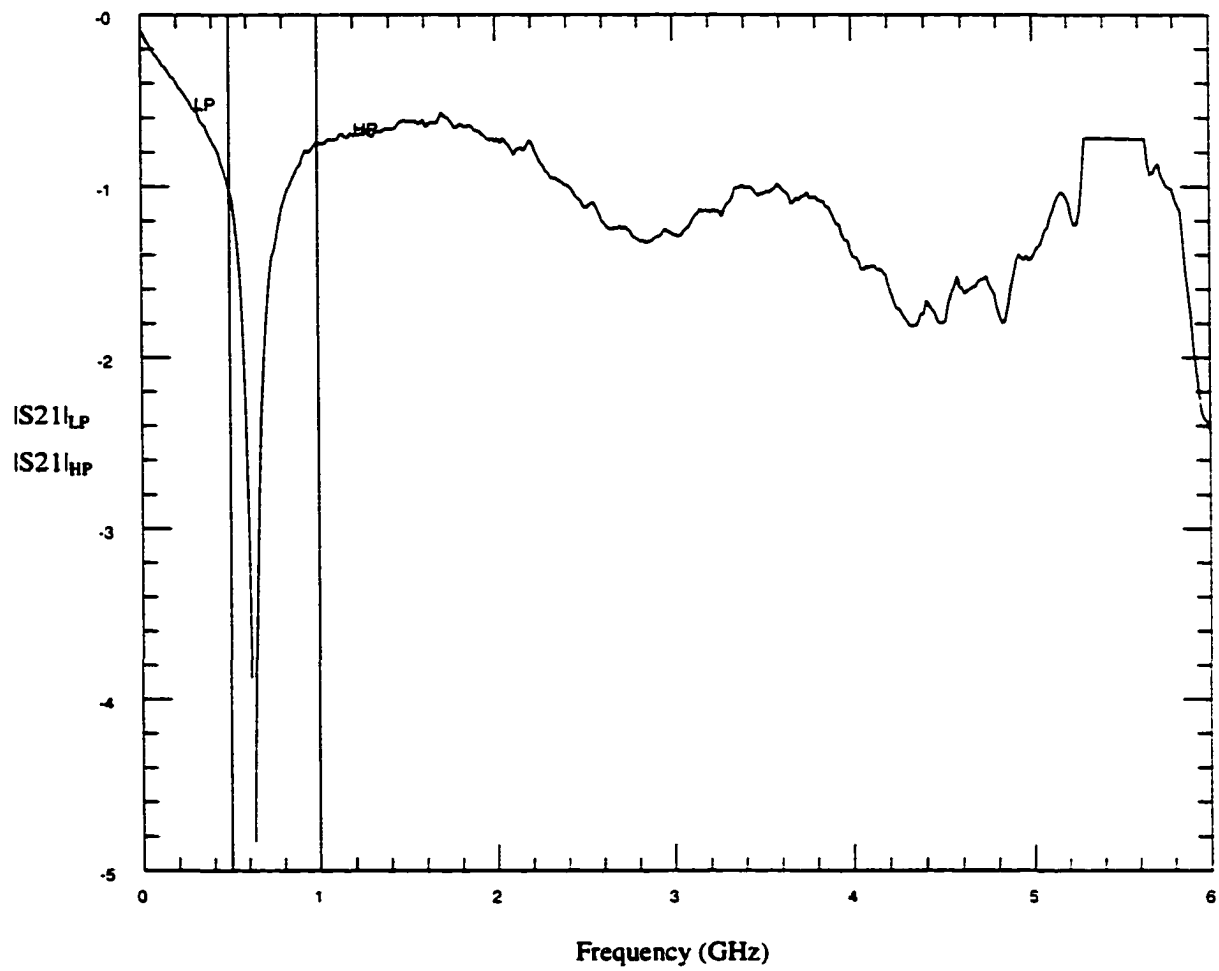

Figure 6-5 Response in the pass bands for the diplexer

6.3 Characteristic of the Frequency Doubler

Relative responses (relative signal levels) of the frequency doubler are shown in Figure 6-6.

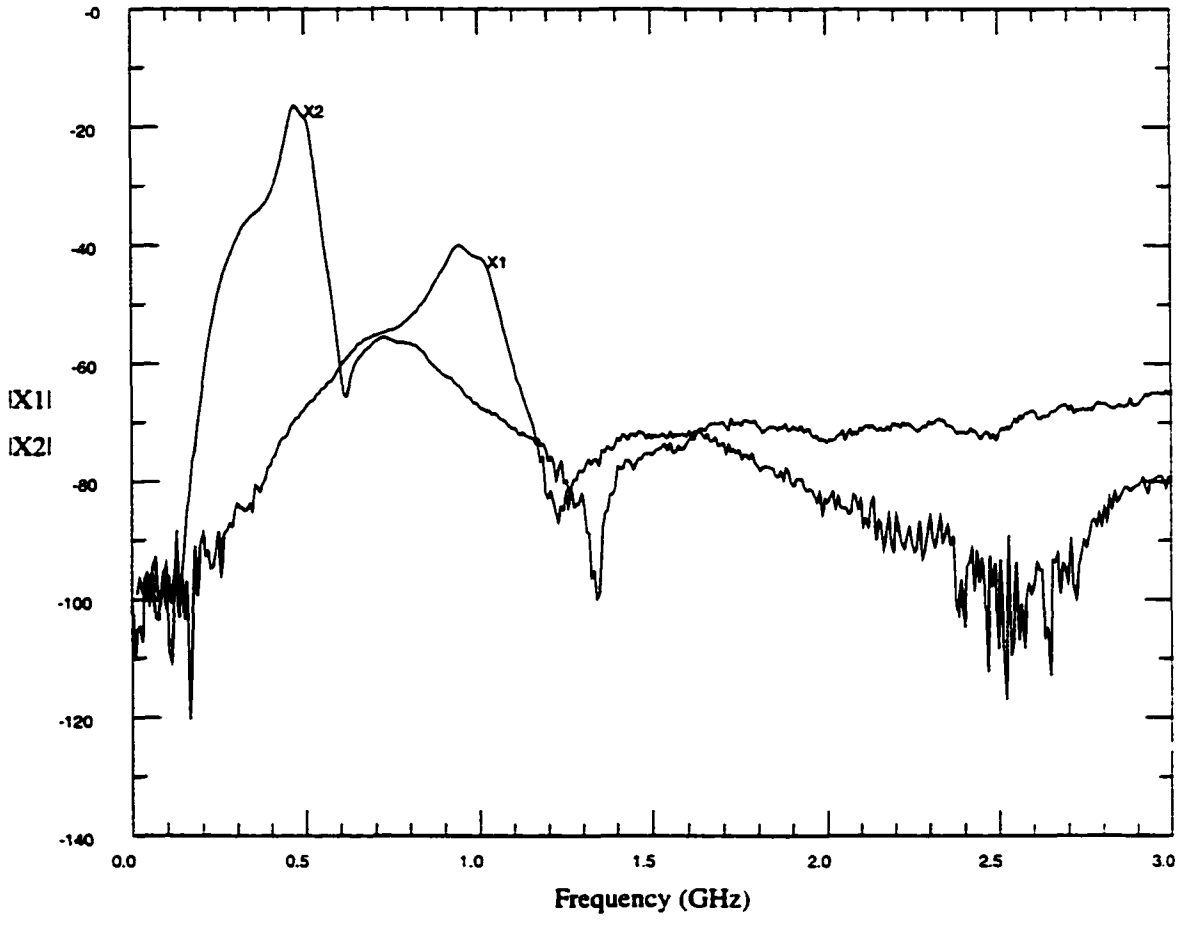

Figure 6-6 Relative responses of the fundamental

signal and the second harmonic signal of the frequency doubler

6.4 Characteristic of the Fixture of the Bipolar Part

S11 and S21 of both halves of the fixture of the bipolar part are shown in Figure 6-7 and Figure 6-8. S11 is the input reflection coefficient and thus indicates the matching characteristic. S21 is the forward transmission coefficient.

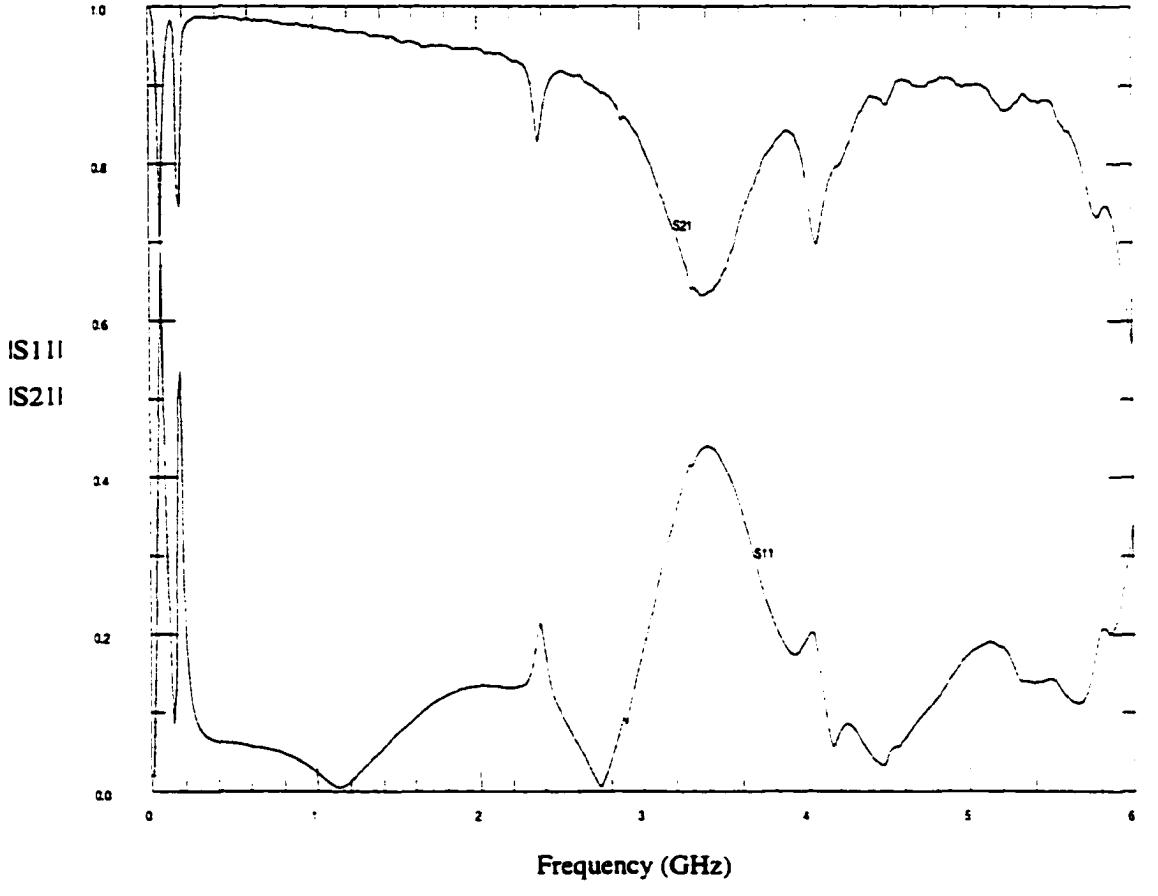

Figure 6-7 Characteristic of the left half of the fixture

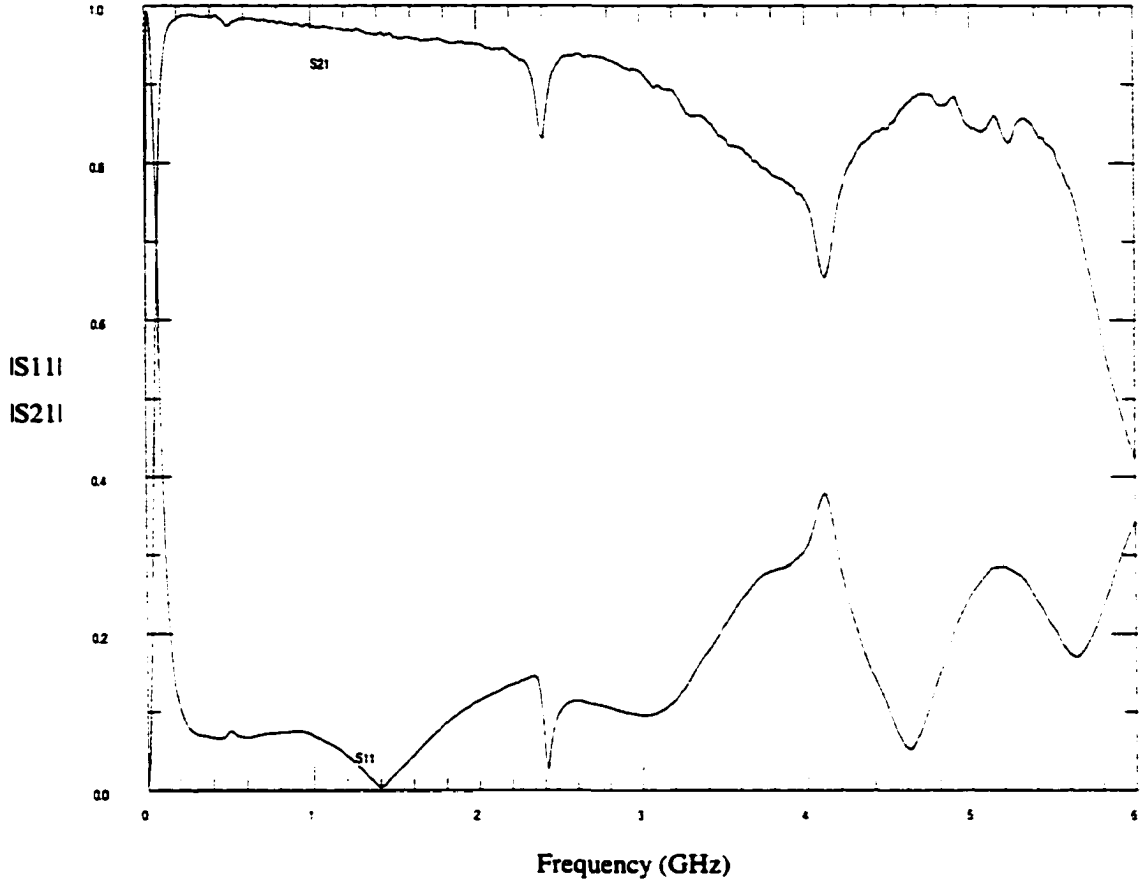

Figure 6-8 Characteristic of the right half of the fixture

6.5 Characteristic of the Fixture of the PHEMT Part

S11 and S21 of the whole fixture of the PHEMT part are plotted in Figure 6-9.

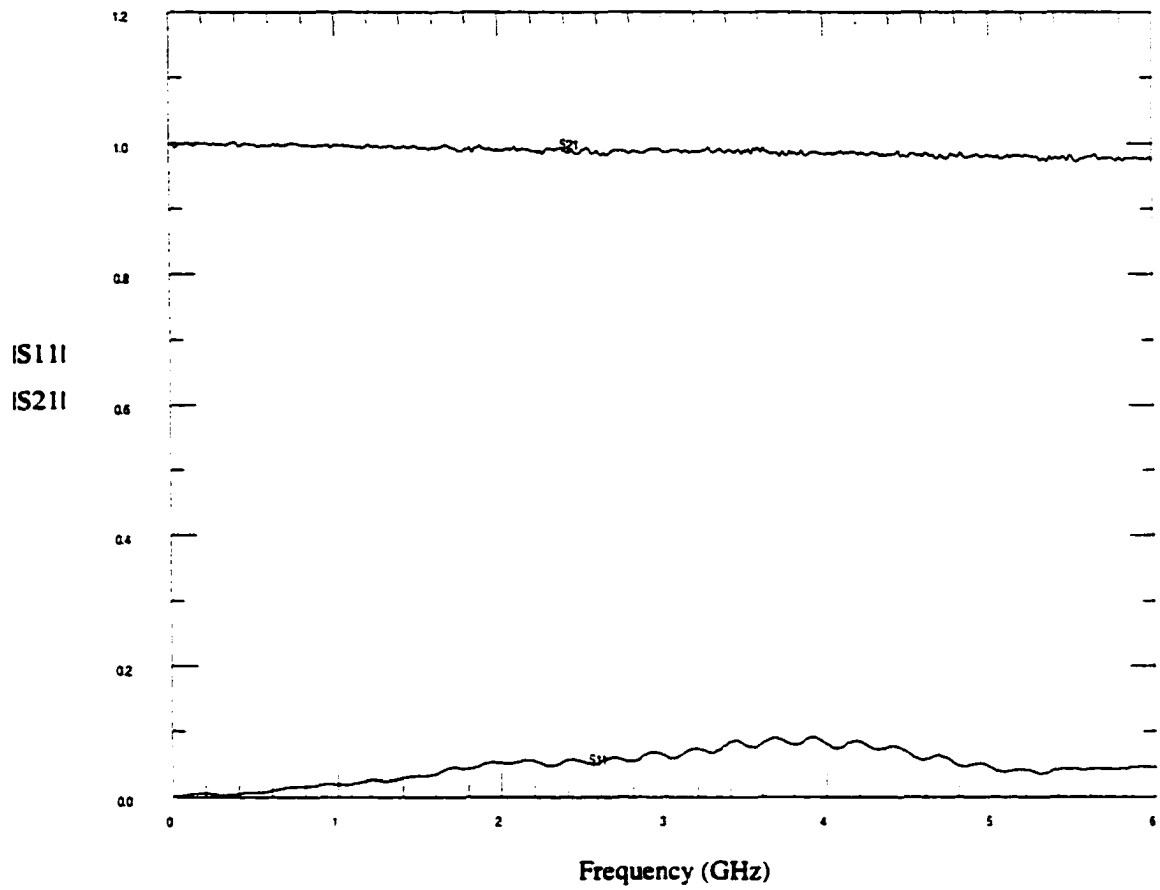

Figure 6-9 Characteristic of the PHEMT fixture

6.6 Coupler File

Table 6-1 Coupler file (part 1)

Frequency (0.5 GHz)				
	Mag(dB)	Ang(deg)	Mag(dB)	Ang(deg)
s11, s12	-24.72	7	-0.13	-109
s13, s14	-26.20	53	-51.91	164
s21, s22	-0.11	-109	-22.13	-45
s23, s24	-53.60	104	-26.45	25
s31, s32	-26.17	53	-52.82	112
s33, s34	-34.40	34	-81.41	113
s41, s42	-51.93	160	-26.46	25
s43, s44	-89.17	-98	-30.03	71
s55, s56	-36.92	125	-0.10	-110
s57, s58	-26.09	52	-55.46	-9
s65, s66	-0.11	-110	-40.36	161
s67, s68	-51.50	-24	-26.18	25
s75, s76	-26.11	52	-51.66	-25
s77, s78	-43.32	96	-73.32	-39
s85, s86	-56.17	-5	-26.16	25
s87, s88	-80.88	-130	-42.66	112
Frequency (1 GHz)				
	Mag(dB)	Ang(deg)	Mag(dB)	Ang(deg)
s11, s12	-31.44	-63	-0.19	145
s13, s14	-21.34	18	-47.76	55
s21, s22	-0.18	145	-28.96	160
s23, s24	-47.16	-39	-21.57	-38
s31, s32	-21.33	18	-46.83	-39
s33, s34	-30.61	29	-85.15	-92
s41, s42	-47.62	59	-21.61	-38
s43, s44	-73.09	129	-28.66	42
s55, s56	-33.76	-147	-0.16	143
s57, s58	-21.26	15	-49.51	-55
s65, s66	-0.19	143	-33.31	-104
s67, s68	-46.43	-143	-21.34	-40
s75, s76	-21.25	15	-46.04	-142
s77, s78	-39.40	-138	-79.91	72
s85, s86	-50.05	-57	-21.31	-40
s87, s88	-78.94	177	-41.19	141

Table 6-2 Coupler file (part 2)

Frequency (1.5 GHz)				
	Mag(dB)	Ang(deg)	Mag(dB)	Ang(deg)
s11, s12	-28.98	23	-0.30	37
s13, s14	-19.85	-19	-48.29	-68
s21, s22	-0.28	37	-21.97	-138
s23, s24	-44.21	180	-20.13	-102
s31, s32	-19.82	-19	-44.25	177
s33, s34	-30.12	-2	-80.21	-164
s41, s42	-48.66	-69	-20.17	-102
s43, s44	-72.50	-93	-29.63	-17
s55, s56	-38.15	37	-0.23	34
s57, s58	-19.68	-23	-42.60	-149
s65, s66	-0.25	34	-54.59	89
s67, s68	-44.25	99	-19.83	-105
s75, s76	-19.69	-23	-44.40	98
s77, s78	-31.52	-176	-78.42	-115
s85, s86	-42.35	-148	-19.78	-105
s87, s88	-71.07	-167	-33.03	152
Frequency (2 GHz)				
	Mag(dB)	Ang(deg)	Mag(dB)	Ang(deg)
s11, s12	-32.65	-89	-0.36	-71
s13, s14	-20.63	-54	-50.66	98
s21, s22	-0.37	-71	-36.30	-160
s23, s24	-43.26	46	-21.07	-166
s31, s32	-20.62	-54	-43.31	48
s33, s34	-31.66	-45	-68.31	-173
s41, s42	-50.73	98	-21.06	-166
s43, s44	-72.93	110	-31.88	-92
s55, s56	-26.40	147	-0.27	-75
s57, s58	-20.35	-60	-40.93	107
s65, s66	-0.27	-75	-27.06	-159
s67, s68	-44.95	-15	-20.54	-170
s75, s76	-20.36	-60	-44.90	-13
s77, s78	-27.22	126	-79.58	-9
s85, s86	-41.32	107	-20.55	-170
s87, s88	-83.91	-170	-30.68	126

Table 6-3 Coupler file (part 3)

Frequency (2.5 GHz)				
	Mag(dB)	Ang(deg)	Mag(dB)	Ang(deg)
s11, s12	-42.82	-65	-0.39	-177
s13, s14	-24.13	-88	-44.07	-71
s21, s22	-0.41	-177	-28.82	-107
s23, s24	-43.51	-70	-24.65	136
s31, s32	-24.17	-88	-43.62	-72
s33, s34	-36.78	-130	-72.61	-60
s41, s42	-43.75	-70	-24.67	136
s43, s44	-69.61	-37	-32.58	168
s55, s56	-31.93	34	-0.27	178
s57, s58	-23.50	-97	-43.51	27
s65, s66	-0.25	178	-31.87	138
s67, s68	-45.22	-101	-23.73	126
s75, s76	-23.46	-97	-45.30	-99
s77, s78	-29.45	94	-71.89	157
s85, s86	-43.60	30	-23.72	126
s87, s88	-72.48	175	-33.19	94
Frequency (3 GHz)				
	Mag(dB)	Ang(deg)	Mag(dB)	Ang(deg)
s11, s12	-27.08	172	-0.42	75
s13, s14	-36.44	-108	-42.64	178
s21, s22	-0.41	75	-21.81	-180
s23, s24	-43.01	-177	-35.49	95
s31, s32	-36.63	-109	-43.03	-178
s33, s34	-33.60	162	-73.97	180
s41, s42	-42.43	179	-35.51	94
s43, s44	-77.07	64	-32.32	105
s55, s56	-31.01	151	-0.28	69
s57, s58	-32.48	-132	-41.59	-30
s65, s66	-0.30	69	-28.36	104
s67, s68	-41.69	170	-33.29	62
s75, s76	-32.58	-133	-41.96	165
s77, s78	-30.23	-117	-85.05	-51
s85, s86	-41.73	-30	-33.29	62
s87, s88	-70.73	95	-37.83	-159

7. BIBLIOGRAPHY

[Nakhla, 1976] M. S. Nakhla and J. Vlach, "A piecewise harmonic balance technique for determination of periodic response of nonlinear systems," IEEE Trans. Circuits and Systems, vol CAS-23, pp. 85-91, February 1976

[Rizzoli, 1988] V. Rizzoli, C. Cecchetti, A. Lipparini and F. Mastri, "General-purpose harmonic balance analysis of nonlinear microwave circuits under multitone excitation," IEEE Trans. Microwave Theory Tech., vol. MTT-36, pp. 1650-1660, 1988

[Gilmore 1991] R. Gilmore and M. Steer, "Nonlinear circuit analysis using the method of harmonic balance," Int. Journal of Microwave and Millimeter-Wave Computer-Aided Engineering, vol. 1, pp. 143-158, April 1991

[Sechi, 1983] F. Sechi, R. Paglione, B. perlman, and J. Brown, "A computer-controlled microwave tuner for automated loadpulll," RCA Review, vol. 44, pp. 566-583, December 1983

[Takayama, 1976] Y. Takayama, "A new load-pull characterization method for microwave power transistors," IEEE MTT-S Int. Microwave Symposium Digest, pp. 218-220, June 1976

[Heymann, 2000] P. Heymann, R. Doerner and M. Rudolph, "Harmonic tuning of power transistors by active load-pull measurement," Microwave Journal, pp. 22-37, June 2000

[Cai, 1998] Q. Cai, J. Gerber and S. Peng, "A systematic scheme for power amplifier design using a multi-harmonic loadpull simulation technique," IEEE MTT-S Int. Microwave Symposium Digest, pp. 161-164, 1998

[Mazumder, 1978] S. R. Mazumder and P. D. van der Puije, "Two-signal method of measuring the large-signal S-parameters of transistors," IEEE Trans. Microwave Theory Tech., vol. MTT-26, pp. 417-420, June 1978

[Tucker, 1981] R.S. Tucker, "RF characterization of microwave power FETs," IEEE Trans. Microwave Theory Tech., vol. MTT-29, pp. 776-781, August 1981

[Maas, 1988] S. Maas, Nonlinear Microwave Circuits. Norwood, MA: Artech House, 1988

[Chua, 1972] L. Chua and Y. Tang, "Nonlinear oscillation via Volterra series," IEEE Trans. Circuits and Systems, vol CAS-29, pp. 150-168, March 1972

[Hu, 1989] Y. Hu, J. Obregon and J. Mollier, "Nonlinear analysis of microwave FET oscillators using Volterra series," IEEE Trans. Microwave Theory Tech., vol. MTT-37, pp. 1689-1693, November 1989

[Teeter, 1993] D. Teeter, J. East, R. Mains and G. Haddad, "Large-signal numerical and analytical HBT models," IEEE Trans. Electron Devices, vol. 40, pp. 837-845, May 1993

[Curtice, 1985] W. Curtice and M. Ettenger, "A nonlinear GaAs FET model for use in the design of output circuit for power amplifiers," IEEE Trans. Microwave Theory Tech., vol. MTT-33, pp. 1383-1393, December 1985

[Ebers, 1954] J. Ebers and J. Moll, "Large Signal Behavior of Junction Transistors," Proceedings of the IRE, vol. 45, pp. 1761-1772, December 1954

[Chang, 1986] F. Chang, "Bipolar transistor models for CAD", Circuit Analysis, Simulation and Design. New York: North-Holland, 1986

[Materka, 1985] A. Materka and T. Kacprzak, "Computer calculation of large signal GaAs FET amplifier characteristics," IEEE Trans. Microwave Theory Tech., vol. MTT-33, pp. 129-134, February 1985

[ADS, v1.50] Advanced Design System, v. 1.50, Hewlett Packard Co.

[Kurokawa, 1965] Y. Kurokawa, "Power waves and the Scattering matrix," IEEE Trans. Microwave Theory Tech., vol. MTT-13, pp. 194-202, March 1965

[Lott, 1989] U. Lott, "Measurement of Magnitude and Phase of Harmonics Generated in Nonlinear Microwave Two-Ports," IEEE Trans. Microwave Theory Tech., vol. MTT-37, pp. 1506-1511, October 1989

[Verspecht, 1995] J. Verspecht, "Accurate on Wafer Measurement of Phase and Amplitude of the Spectral Components of Incident and Scattered Voltage Waves at the Signal Ports of a Nonlinear Microwave device," IEEE MTT-S Int. Microwave Symposium Digest, pp. 1029-1032, 1995

[Barataud, 1999] D. Barataud, " Measurement and Control of Current/Voltage Waveforms of Microwave Transistors Using a Harmonic Load-Pull System for the Optimum Design of High Efficiency Power Amplifiers," IEEE Trans. Microwave Theory Tech., vol. MTT-48, pp. 835-842, August 1999

[Browne, 1991] J. Browne, "Transition Analyzer Scans Amplitude and Phase of 40 GHz Pulses," Microwaves&RF, pp. 150-157, March 1991

[Kompa, 1990] G. Kompa and F. V. Raay, "Error-Corrected Large Signal Waveform Measurement System Combining Network Analyzer and Sampling Oscilloscope Capabilities," IEEE Trans. Microwave Theory Tech., vol. MTT-38, pp. 358-365, April 1990

[Sipila, 1988] M. Sipila, K. Lehtinen and V. Porra, "High-Frequency Periodic Time-Domain Waveform Measurement System," IEEE Trans. Microwave Theory Tech., vol. MTT-36, pp. 1397-1405, October 1988

[Weber, 2001] R. J. Weber, Introduction to Microwave Circuits: Radio Frequency and Design Applications, IEEE Press, 2001

[Weber, 2000] R. J. Weber, "Half Frequency Characterization – Bipolar Part", Interim Report for Rockwell International, August 2000

[Linville, 1961] Linville and Gibbons, Transistors and Active Circuits, McGraw-Hill Book Company, Inc., 1961

[Rollet, 1962] J. Rollet, "Stability and Power Gain Invariants of Linear Two-Ports," IRE Transactions on Circuit Theory, vol. CT-9, pp.29-32, 1962

[Weber, 1987] R. J. Weber, RF/Microwave Class, University of Iowa, Iowa City 1987

[Weber, 1990] R. J. Weber, "Some Design Considerations for L-Band Power MMICs," Proceedings RF Expo EAST, pp. 187-199, November 1990

[Edwards, 1992] M. L. Edwards and J. H. Sinsky, "A New Criterion for Linear Two-Port Stability Using a Single Geometrically Derived Parameter," IEEE Trans. Microwave Theory Tech., vol. MTT-40, pp.2303-2311, December 1992